LBL-11311 c.2

Lawrence Berkeley Laboratory
UNIVERSITY OF CALIFORNIA

ENERGY & ENVIRONMENT DIVISION

APPLIED RESEARCH IN LASER SPECTROSCOPY AND ANALYTICAL TECHNIQUES

Chapter from the Energy and Environment Division Annual Report 1979

October 1980

TWO-WEEK LOAN COPY

This is a Library Circulating Copy which may be borrowed for two weeks. For a personal retention copy, call Tech. Info. Division, Ext. 6782.

RECEIVED
LAWRENCE
BERKELEY LABORATORY

DEC 11 1980

LIBRARY AND
DOCUMENTS SECTION

LBL-11311 c.2

Prepared for the U.S. Department of Energy under Contract W-7405-ENG-48

DISCLAIMER

This document was prepared as an account of work sponsored by the United States Government. While this document is believed to contain correct information, neither the United States Government nor any agency thereof, nor the Regents of the University of California, nor any of their employees, makes any warranty, express or implied, or assumes any legal responsibility for the accuracy, completeness, or usefulness of any information, apparatus, product, or process disclosed, or represents that its use would not infringe privately owned rights. Reference herein to any specific commercial product, process, or service by its trade name, trademark, manufacturer, or otherwise, does not necessarily constitute or imply its endorsement, recommendation, or favoring by the United States Government or any agency thereof, or the Regents of the University of California. The views and opinions of authors expressed herein do not necessarily state or reflect those of the United States Government or any agency thereof or the Regents of the University of California.

APPLIED RESEARCH IN LASER SPECTROSCOPY AND ANALYTICAL TECHNIQUES

FY 1979

The research reported in this volume was undertaken during FY 1979 within the Energy & Environment Division of the Lawrence Berkeley Laboratory. This volume will comprise a section of the Energy & Environment Division 1979 Annual Report.

CONTENTS

Applied Physics and Laser Spectroscopy Research
N. Amer, N. Bergstrom, J. Costello, R. Gerlach, W. Jackson, R. Johnson, S. Kohn, C. Rosenblatt, D. Wake, and Z. Yasa 9-1

Operation of a Gas Chromatograph/Mass Spectrometer for the Identification of Components in Fossil Energy and Environmental Samples
A. Newton and W. Walker. 9-15

Development and Application of X-Ray Fluorescence Analytical Methods
R. Giauque 9-17

Survey of Instrumentation for Environmental Monitoring
M. Quinby-Hunt, Y. Agrawal, C. Chen, R. McLaughlin, G. Morton, D. Murphy, and A. Nero. 9-18

Extraterrestial Cause for Cretaceous-Tertiary Extinction: Experiment and Theory
L. Alvarez, W. Alvarez, F. Asaro, and H. Michel. 9-19

Precise Analysis for Better Understanding of Guatemalan Obsidian
F. Stross, F. Asaro, and H. Michel 9-23

APPLIED RESEARCH IN LASER SPECTROSCOPY AND ANALYTICAL TECHNIQUES

APPLIED PHYSICS AND LASER SPECTROSCOPY RESEARCH*

N. Amer,† N. Bergstrom, J. Costello, R. Gerlach, W. Jackson, R. Johnson, S. Kohn, C. Rosenblatt, D. Wake, and Z. Yasa

OVERVIEW

The research philosophy of our group is to apply advanced laser spectroscopy and condensed matter physics to energy and environmental problems. With the narrow linewidth and the tunability of lasers, unsurpassed sensitivity and specificity can be achieved in detecting trace contaminants of the atmosphere. The advanced state of condensed matter physics enables us to apply such knowledge to energy production processes and to test novel methods for energy conversion, such as photovoltaic devices, superionic electrical energy storage devices, and the extraction of oil from oil shales with lyotropic liquid crystal emulsifiers.

LASER PHOTOACOUSTIC MEASUREMENTS & CHARACTERIZATION

Laser photoacoustic spectroscopy provides a very powerful tool for the detection of trace contaminants in air and water as well as a means for investigating the fundamental properties of gaseous, liquid, or solid phases of matter. One of our goals is to develop ultrasensitive multiparameter elemental and molecular detectors for the characterization of pollutants released in the process of energy production and utilization. Another aim is to maintain a state-of-the-art capability in photoacoustic detection by fully understanding the physics of this technique. Concurrent with these efforts, we are active in developing new or modified laser systems compatible with our particular needs. Below we report on some of our results.

A Resonant Spectrophone for Intracavity Use**

As acoustically resonant spectrophones began to be used in conjunction with lasers for trace gas analysis, it was quickly realized that their already high sensitivity to weak optical absorption could be further enhanced by use of a multipass geometry to increase the amount of absorbed power.[1,2] A comparable increase in absorbed power could be achieved by placing the spectrophone inside the cavity of a laser, where the increase is due not to an increased path length but to a higher beam power available for absorption.

A principal obstacle to intracavity operation is that for conventional resonant spectrophone designs, in which the beam passes through the windows at normal incidence, the window reflection losses impair operation of the laser. A further problem, not unique to intracavity spectrophones, is that if the beam enters and leaves the cell at points of high pressure amplitude for the mode being excited, as is the case when the beam passes directly down the center of a cylindrical cell and a radial mode is excited, any window absorption can give rise to a spurious background signal resulting from window heating. The first problem can be alleviated by antireflection coating the windows, but single-layer AR coatings are usable over only a limited range of wavelengths. It would be more desirable to have the beam enter and leave at Brewster's angle, since for many commonly used optical materials, such as fused silica and sodium chloride, Brewster's angle is nearly constant over a wide range of wavelengths, and tolerance to small variations is large since reflectivity varies quadratically with small deviations from Brewster's angle. Window heating can be alleviated by placing the windows at nodes of the mode being excited. Somewhere inside the cell, however, the beam must pass through a region where the mode has a high amplitude in order to excite that mode efficiently.

For a spectrophone to be used for monitoring ambient air, it would be desirable to eliminate the windows altogether.[3] This would permit continuous sampling by inducing a slow flow of air through the cell. Absence of windows certainly solves the optical insertion loss problem, yet it can greatly degrade the quality factor (Q) of the acoustical cavity resonance. Again, the solution is to let the beam enter and leave the cell at pressure nodes, where the holes will constitute a minimal perturbation.

Our spectrophone design, based on the above considerations, is shown in Fig. 1. As for all cylindrical acoustical resonant cells, the pressure amplitude for the first radial mode is a maximum

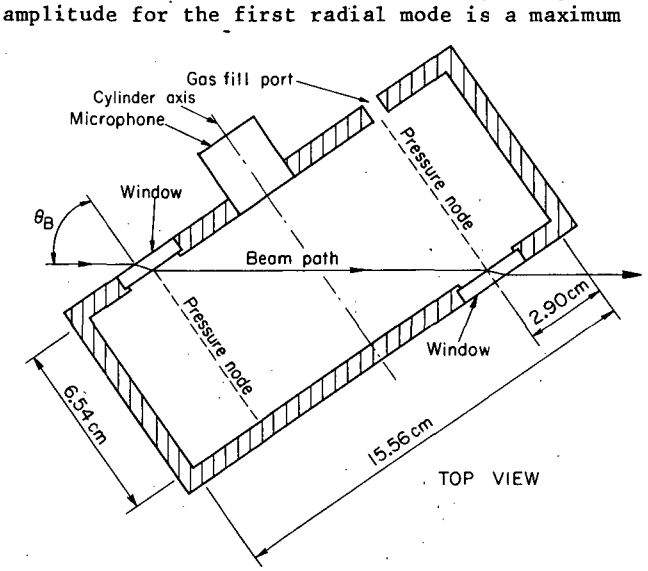

Fig. 1. Brewster Window Spectrophone (top view). (XBL 803-3125)

†Group Leader

along the center axis of the cylinder, passes through zero about 2/3 of the way out to the wall, and reaches a negative extremum at the wall. The beam enters our cell through a window mounted virtually flush with a flat end wall, passes diagonally through the center of the cell, and exits through a window on the other flat wall. The entry and exit points are chosen to lie on a node of the first radial mode. For the beam to pass through the windows at Brewster's angle, the ratio of cell radius to length must be 0.7967 times the refractive index of the window material; thus for n=1.5, R/L=1.19.

The microphone is centered directly on the cell axis. This has two advantages. First, the flat microphone face mounts approximately flush with the flat end wall of the cylinder and does not perturb the cell geometry as it would on a cylindrical wall. Second, the microphone is now at the absolute maximum of the first radial mode, where the pressure amplitude is 2-1/2 times larger than at the cylindrical wall, the usual microphone location.

The same design is applicable to windowless operation. However, there is no longer a constraint on the ratio R/L, and it is therefore desirable to make the ratio smaller. Smaller beam entrance holes can be used without aperturing the beam, the importance of viscous losses on the flat end walls is reduced, and the first radial resonant frequency is moved farther from the relatively broad first longitudinal resonance, which is strongly excited by ambient room noise.

We have investigated the performance of the spectrophone using a calibration mixture of 54 ppm of ethylene in nitrogen and using pure nitrogen to determine background signal levels. The light source for these experiments was a current-modulated CO_2 laser tuned to the P(14) line in the 10.6 μm band, for which the absorption coefficient of ethylene is known to be about 31 $atm^{-1}cm^{-1}$. The R/L ratio for our design was appropriate for NaCl Brewster windows, but we also tried operating the cell without any windows. Our investigations established the following:

- The Q of the first radial resonance at 2700 Hz is 560 when the cell is operated with windows. Removing the windows only decreases the Q to 509.

- The calibration of the cell was 26.5 volts per watt per cm of absorbed power, or in terms of pressure units, 241 Pa per watt per cm.

- The calibration does not depend very sensitively on the precise alignment of the beam through the cell, so misalignments can be tolerated as far as calibration is concerned.

- The coherent background signal due to window heating and to scattered or reflected light heating the cell walls is indeed minimized by the geometry chosen. As the beam deviates from its intended path through the cell, background signal increases, but shows a sufficiently broad minimum as a function of the various pertinent geometrical variables so that, again, alignment of the beam is not ultracritical. Also, variations of the beam polarization from the plane of incidence by a few degrees can be tolerated. The background is equivalent to an absorption coefficient of 2.1 x 10^{-7} cm^{-1}, or an ethylene concentration of 6.6 parts per billion.

- The random noise level when the spectrophone is operated with windows is equivalent to an absorption coefficient which can be found by multiplying 3.8 x 10^{-8} W cm^{-1} $Hz^{-1/2}$ times the square root of the bandwidth divided by the laser power. For intracavity operation with a 1 Hz bandwidth this could be made very small, 7.5 x 10^{-10} cm^{-1}, equivalent to 25 parts per trillion of ethylene. In this case, however, sensitivity would be limited by the coherent background signal.

- Windowless operation is limited in sensitivity by ambient room noise. For the cell dimensions used, the first radial mode lies close to the first longitudinal mode, which has a low Q and is strongly excited by room noise.

In conclusion, our new spectrophone design offers low insertion loss making possible intracavity operation, high sensitivity, and low background signal. These features should make it attractive for a wide variety of gas analysis and spectrophone investigations, especially where broadly tunable lasers are used.

FOOTNOTE AND REFERENCES

**Complete version accepted for publication in Applied Physics (1980).

1. C. F. Dewey, R. D. Kamm and C. E. Hackett, Appl. Phys. Lett. 23, 633 (1973).

2. E. Max and L. G. Rosengren, Opt. Commun. 11, 422 (1974).

3. Another design for a windowless resonant spectrophone, differing drastically from ours, was presented by S. Shtrikman and M. Slatkine, Appl. Phys. Lett. 31, 830 (1977).

Piezoelectric Photoacoustic Detection: Theory and Experiment*

Introduction

When an intensity modulated light beam is absorbed by a medium, part of all of the excitation energy is converted to thermal energy. In "conventional" photoacoustic spectroscopy, the generated heat is coupled to an optically nonabsorbing gas and the time-dependent pressure fluctuation is detected with a microphone. The universal applicability of this approach to gases,[1-6] liquids,[7-9] solids,[10-14] and aerosols[15,16] makes it a versatile detector scheme. Nevertheless, this approach suffers from certain crucial limitations, particularly in

the case of condensed matter samples. Perhaps the most serious restrictions are the narrow bandwidth of the microphone response, the relatively complex nature of the heat transfer process from the sample to the gas, and the inability to perform experiments at low pressures. Furthermore, saturation problems limit the usefulness of this technique in the case of strong optical absorption.

An alternative photoacoustic detection scheme is to attach a piezoelectric transducer (PZT) directly to the sample. The absorption-induced heating causes the sample to develop thermal stresses and strains which are transmitted to the sample surface. The attached PZT converts these stresses and strains to a measurable voltage.

This approach has several advantages over gas cell photoacoustics. PZTs have a wide frequency response range from a few Hz to many MHz, and they can be used over a broad range of temperatures and pressures. Since the sample-PZT configuration is compact and rugged, it is useful in space-limited experiments (e.g., inside a low temperature optical dewar). Because the PZT responds to absorption of radiation by the entire sample, not merely within a thin thermal length, the complicated solid-gas coupling is eliminated. Furthermore, as we shall demonstrate, piezoelectric-photoacoustic spectroscopy (PZT-PAS) is a very sensitive means for measuring absorption coefficients as low as 10^{-5} cm^{-1} for a 1 W laser, and does not show saturation for $\alpha\ell$ as high as 10.

Below, we develop a computationally tractable thermoelastic theory for piezoelectric photoacoustic detection at low modulation frequencies. This theory was tested experimentally with samples whose thermal and optical properties cover a wide range. We find that our theoretical treatment quantitatively accounts for the observed magnitude and phase of the signal, and describes its functional dependence on modulation frequency, absorption coefficients, and thermal properties of the sample.

Theory

An outline of the steps of the theory of PZT-PAS is shown in Fig. 2. The signal is generated when a beam of light is incident on an absorbing solid. The temperature of the illuminated volume increases, leading to the expansion of that region and the outflow of heat (Fig. 3a). The expansion of the central region causes displacement of the sample surface by two separate mechanisms. First, the enlargement of the central region causes the expansion of both surfaces of the sample (Fig. 3a). Second, in the case of strongly absorbing samples, the heat in the illuminated region decays spatially through the thickness of the sample (Fig. 3b). Consequently, the front portion of the sample expands more than the rear, resulting in a bending of the sample. Such bending compresses the rear surface of the solid and opposes the general expansion shown in Fig. 3a. The bending also causes expansion of the front surface, thus adding to the expansion described in Fig. 3a. This displacement of the sample surface is then sensed by the transducer (Fig. 4a) causing a voltage to develop in the z-direction between the two surfaces of the PZT.

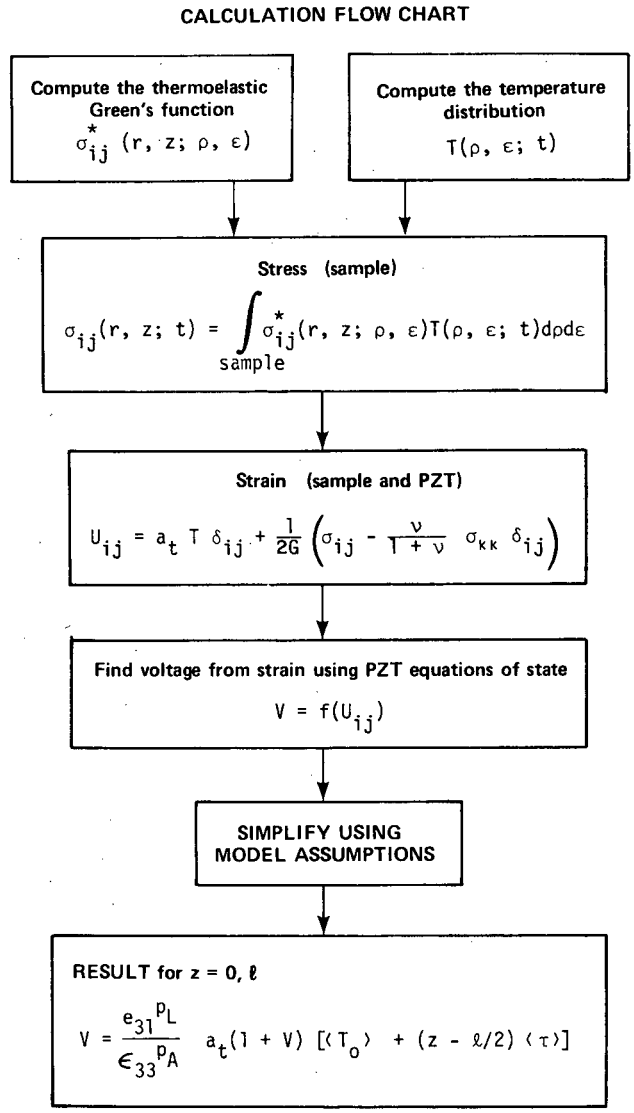

Fig. 2. Flowchart showing steps in the calculation. The symbols are defined in the text.

(XBL 797-2310)

Detector Geometry. Consider the geometry shown in Figs. 4a and 4b. We treat two cases: (1) optically thick samples, where the light beam is not transmitted and the PZT is a slab covering the entire back surface of the solid (Fig. 4b), and (2) optically thin samples, where the PZT is an annulus and is located on either side of the solid (Fig. 4a). As will be shown, the nature of the generating strain in the latter case is dependent upon the side on which the transducer is located.

Assumptions of the Theory. To simplify the problem, we assume the solid to be an isotropic, infinite, elastic layer. This approximation is reasonable since a focused light beam is typically much smaller than the sample dimensions. We also assume that the sample responds as if its boundaries

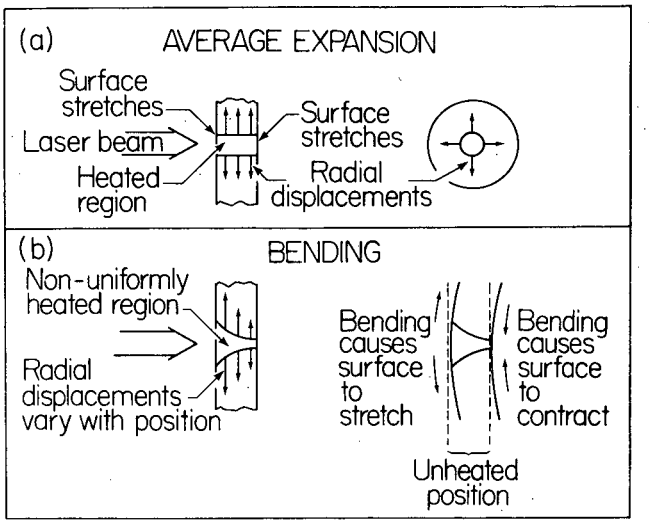

Fig. 3. Sources of surface strain. Transducer may be attached to either side of the sample.
(XBL 797-2315)

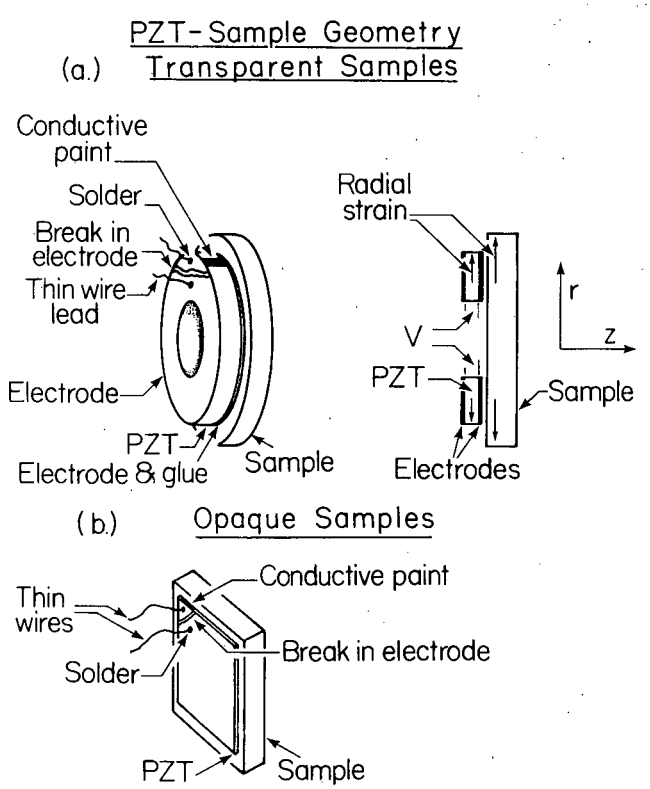

Fig. 4. Transducer-sample geometry.
4a) Configuration used for transparent samples.
4b) Configuration for opaque samples.
(XBL 797-2316)

were free from stress. This is plausible since the transducer is much thinner than the sample. In fact, for a transparent solid (Fig. 4a) the sample is free in its central region.

Predictions of the Theory. By calculating the temperature distribution in the sample and the corresponding induced strain, we were able to calculate the potential difference V generated by the PZT as a result of stress induced in the sample itself from the absorption of the electromagnetic radiation. We show that such a potential difference V is given by

$$V \simeq \frac{e_{31}^{P} L\, a_t}{\varepsilon_{33}^{P} A} (1+\nu) \left[\langle T_o \rangle + (z-\ell/2) \langle \tau \rangle \right]_{z=0,\ell} \qquad (1)$$

where e_{31}^{P} and ε_{33}^{P} are the piezoelectric and dielectric constants of the PZT, L is its thickness, and A is its area. a_t is the expansion coefficient of the sample, ν is Poisson's ratio, $\langle T_o \rangle$ is the in-plate displacement due to the average temperature T_o. The second term represents the sample buckling due to the average temperature gradient τ. When the transducer is on the laser side of the sample, the average term and the buckling term add since $\langle \tau \rangle < 0$. When the transducer is away from the laser, the terms subtract.

Implications of the Theory. Physically, the implications of Eq. (1) are more apparent if one considers specific cases. In the following cases, $l_t = (2\lambda/\omega)^{1/2}$ is the thermal length, $l_o(=1/\alpha)$ is the optical length of the sample, and, for simplicity, we have neglected surface conduction from the sample to the ambient air.

Case 1: For thermally and optically thick samples with the transducer located at $z=\ell$, we have with $\ell \gg l_t$ and $\ell \gg l_o$

$$V \simeq -\frac{2M\, Pa_t}{i\omega\ell(\rho C)_{sample}} \qquad (2)$$

where

$$M = \frac{e_{31}^{P} L}{\varepsilon_{33}^{P} A} \frac{2(1+\nu)}{\pi}$$

Case 2: For thermally thin but optically thick samples ($l_t \gg \ell \gg l_o$), we have

$$V \simeq \frac{M\, Pa_t}{i\omega\ell(\rho C)_{sample}} \qquad (3)$$

again when the transducer is located at $z=\ell$.

Case 3: For thermally thick but optically thin samples ($l_o \gg \ell \gg l_t$), we have

$$V \simeq \frac{M\,Pa_t}{i\omega\ell(\rho C)_{sample}} \left\{1 - e^{-\alpha\ell} \pm \frac{6}{\ell\alpha}\left[\left(1 - \frac{\ell\alpha}{2} - e^{-\alpha\ell}\left(1 + \frac{\ell\alpha}{2}\right)\right)\right]\right\} \quad (4)$$

where the negative sign applies for ($z=\ell$) the case when the transducer is away from the laser beam, and the positive sign is applicable when the transducer is towards the laser ($z=0$).

From the above cases we find the general form of the signal is

$$V \propto M\, a_t \frac{1}{\rho C} \frac{P}{\omega} ,$$

P/ω is the energy deposited per cycle, $1/\rho C$ converts the energy to a temperature, a_t transforms the temperature rise to a strain, and M is a voltage for a given strain.

Based on this theory, the following predictions are made.

1) The signal amplitude is proportional to the reflection-corrected incident power.

2) The signal amplitude is related to the material parameters through the quantity $a_t(1-R)/(\rho C)_{sample}$. Note that the signal does not depend on Young's modulus or on the conductivity κ directly. The conductivity affects the signal as a result of its effect on the thermal length.

3) The signal amplitude has a $1/\ell$ dependence; hence thin samples tend to yield higher signals.

4) The signal has approximately $1/\omega$ dependence. The exact theory shows that the frequency dependence closely approximates a $1/\omega^{0.9}$ dependence for thick metal samples.

5) The phase for metal data undergoes a 180° phase shift as the thermal length becomes smaller than the sample thickness.

6) For small values of α, the photoacoustic signal is directly proportional to α. For high values α, the position of the PZT with respect to the direction of the incoming beam ($z=0$ or $z=\ell$) yields significantly different results. When the transducer is away from the laser beam ($z=\ell$), as α increases, the signal should decrease, eventually passing through zero and changing signs at higher values of α. On the other hand, when the transducer is attached to the sample surface towards the laser beam ($z=0$), it is predicted that the signal will show little saturation until α reaches very high values.

Experimental Verification of the Theory

The predictions of our theory were tested experimentally for solids with a wide range of optical and thermal properties. The samples used were tungsten, tantalum, copper, glass coated with black paint, and didymium glass. The piezoelectric transducers (type 5502 lead zirconium titanate alloy) were obtained from Channel Industries and electrodes were attached to them with low temperature solder. For opaque samples (Fig. 4b), a 0.01 x 0.8 x 0.8 cm PZT slab was used; for optically thin samples (Fig. 4a), PZT annuli were employed to minimize the scattering of the exciting light on the transducer itself. After testing several types of adhesive, we chose to employ Eastman 910[17] and a low viscosity epoxy[18] for the work reported below. Our experimental apparatus is shown in Fig. 5.

Verification of $1/\omega$ Dependence. Equation (2) predicts that the amplitude of the photoacoustic signal is approximately inversely proportional to the modulation frequency of the exciting light. By varying the chopping frequency using a computer, we found this to be the case for all of our samples over the modulation range tested (5-2000 Hz) as shown in Fig. 6.

Power Dependence of the Signal. The power dependence of the observed signal was verified by attenuating the intensity of the laser beam with calibrated filters. For various samples we found the signal to depend linearly on the power for over six orders of magnitude. The minimum power we could detect was 0.1 μW for a signal to noise ratio of one. This is in agreement with our predictions. By using a copper sample and continuously varying the wavelength of a dye laser, we verified the prediction that the signal is a linear function of the incident power when corrected for the reflectivity of the sample.

Signal Dependence on the Optical Absorption Coefficient. The absorption bands of the didymium glass around the 5800 Å region were used to test the theoretical prediction of the signal dependence on the absorption coefficient. The sample absorption was measured simultaneously by transmission and by photoacoustics on two identical samples (Fig. 5). The experiments were performed for the transducer away and towards the laser beam. The agreement between the theory and the experimental results is good, as can be seen in Figs. 7-8. When the transducer is away from the beam ($z=\ell$), the

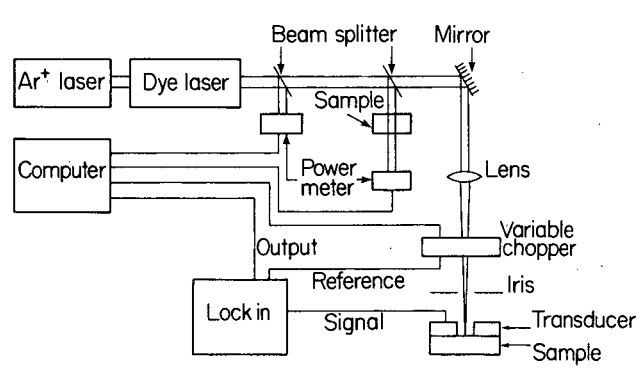

Fig. 5. Experimental apparatus. The two samples are identical. (XBL 797-2317)

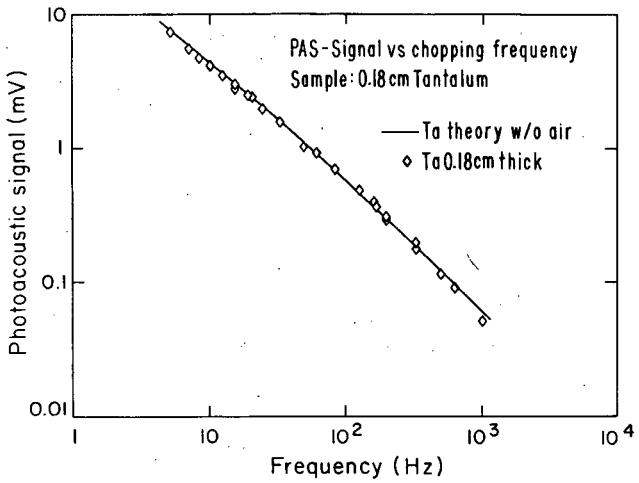

Fig. 6. PAS signal vs. modulation frequency. Both full theory (no thermal or optical length approximations are made) and experiment show slightly less than a $1/\omega$ dependence $(1/\omega^{+0.9})$. (XBL 797-2312)

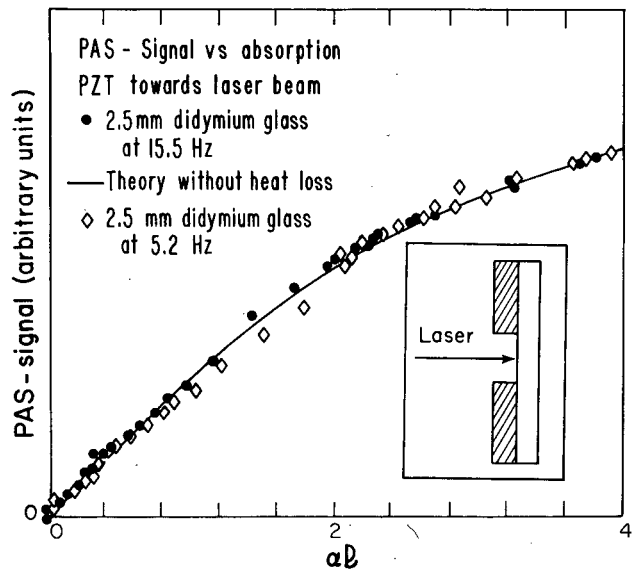

Fig. 8. PAS signal vs. $\alpha\ell$. (XBL 797-2308)

relationship between the photoacoustic signal and optical absorption is highly nonlinear. The signal goes to zero at $\alpha\ell = 2$, where the compression due to the bending equals the expansion due to the heating. In Fig. 7 we show the abrupt 180° phase shift by a negative amplitude. When the tranducer is towards the laser beam (z=0) (Fig. 8), the bending and expansion terms add, increasing the observed signal. There is no saturation until high values of absorption.

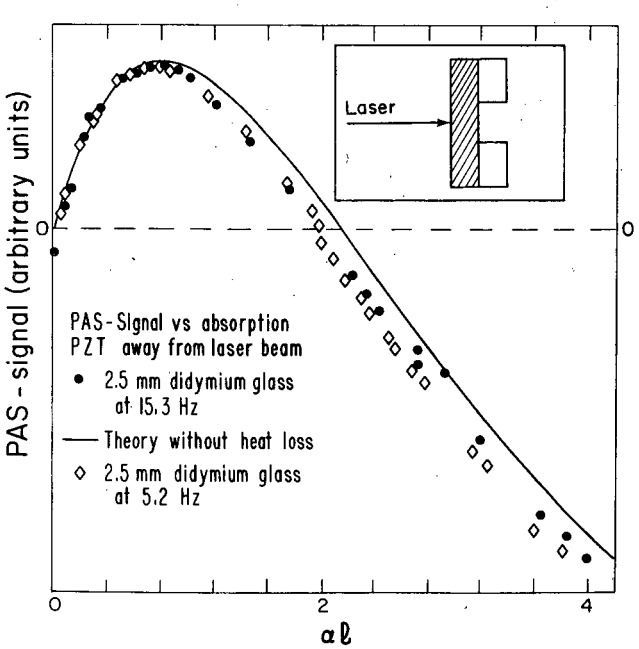

Fig. 7. PAS signal vs. $\alpha\ell$. Inset shows direction of incident light in relation to the transducer. At $\alpha\ell \sim 2$, the phase undergoes a 180° phase shift which is indicated by making the signal amplitude negative. (XBL 797-2309)

The Dependence of Signal on Sample Thickness. To test the $1/\ell$ (Eq. 2) dependence, we varied the thickness by using varying lengths of black coated glass rods. We found that the signal exhibits approximately a $1/\ell$ dependence.

Signal Dependence on the Thermal Properties of the Sample. We have compared the relative magnitudes of the photoacoustic signal obtained from aluminum, tantalum, and copper samples of identical thickness. Although the results are complicated by uncertainties concerning the reflectivity of the samples, the relative values are in agreement with the predictions. The experimental ratio of tungsten (which has a high E) to tantalum is smaller than predicted. However, the experimentally obtained tungsten signal is smaller than that obtained for tantalum, as is qualitatively predicted by our theory.

The phase of the metal samples shows the predicted 180° phase shift at the predicted frequencies. When the thermal diffusion length is on the order of the sample thickness, the phase shifts. Consequently, because copper has a longer thermal diffusion length, the phase shifts at a higher frequency than tungsten.

We also point out that the absolute theoretical magnitudes of the signal are within a factor of 2 of experimental values. Part of the discrepancy is due to greater absorption than was assumed in the theory. The greater absorption results from surface irregularities and contaminants. Finally, we verified that to within 5% the signal does not depend on the beam radius.

Having tested the theory on a variety of samples with a wide range of thermal and optical properties, we have found good agreement. Consequently, we believe that the theory is useful for quantitative calculations of the expected signal.

Noise Analysis and Noise Equivalent Power

We next analyze the sources of noise and estimate a total noise equivalent power (NEP) for our detector. This discussion identifies factors which limit the sensitivity and serves as a guide for designing an optimized PAS-PZT detector. The noise factors we have considered are electronic noise, material dielectric loss noise, DC leakage noise, Brownian motion of the detector, and thermal noise. The first two are the most important, although DC leakage noise can become significant if the detector is improperly constructed.

Electronic Noise. Since the PZT is a high impedance device, the preamp should contain an FET front end. Consequently, we follow the approach of Van der Ziel[19] and Byer[20] for constructing a noise equivalent circuit including an FET. One can neglect R_{dc}, R_{ac} (providing no low resistance path shunts the transducer), and C_a as far as their effect on the impedance of the network. Furthermore, since one is typically operating at a frequency such that $1/\omega C \ll R_{inp}$, the total impedance of the network is $Z = 1/i\omega C$. The rms noise voltage due to the amplifier is given by:

1) $V_I = i_n\,|Z|\Delta f^{1/2}$ from the current noise

2) $V_V = e_n \Delta f^{1/2}$ from the voltage noise

where

$i_n^2 = 2eI_g$

$e_n^2 = (8k_BT/3g_m)\,(1+f_o/f) + (4k_BT)/R_L\,gm^2$

I_g - gate leakage noise

g_m - FET transconductance

f_o - 1/f noise corner frequency

R_L - load resistor

T - amplifier temperature

Δf - lock-in bandwidth.

Since the signal for all cases has the form

$$V = J\,P\,|Z|/\ell$$

where

$$J = e_{31}^P\,a_t(1+\nu)/(C\rho)_{sample}; \qquad Z = 1/\omega C = L/\omega\varepsilon_{33}^P A$$

we get the contributions to the NEP,

$$(NEP)_I = i_n\,\ell/J \tag{5}$$

$$(NEP)_V = e_n\ell\,\varepsilon_{33}^P\,A/JL \tag{6}$$

At low frequencies since $e_n \sim 1/\omega^{1/2}$. Then $(NEP)_V \propto \omega^{1/2}$.

PZT Material Noise Sources. The dielectric loss and leakage noise contributions are

$$(NEP)_D = \ell/J\left(\frac{4k_BT\omega\;\;\varepsilon_{33}^P A\,\tan\delta}{L}\right)^{1/2} \tag{7}$$

and

$$(NEP)_{DC} = \ell/J\left(\frac{4k_BT\;\;\sigma A}{L}\right)^{1/2} \tag{8}$$

where $\tan\delta$ is the dielectric loss tangent and σ is the volume resistivity.

Fundamental Noise Sources. The NEP due to fluctuations of the temperature of the transducer is

$$(NEP)_{thermal} = \frac{(4k_B\,g_H)^{1/2}\;T\rho\,\ell}{(\rho C)_{PZT}\;LJ} \tag{9}$$

and the NEP due to Brownian motion is approximately

$$(NEP)_{Brownian} = \left(\frac{4k_B\;TA\ell\omega\;\;e_{31}^P}{L^3Q\rho_{PZT}\;\omega_o^3 J}\right)^{1/2} \tag{10}$$

where g_H is the thermal conductance with the surroundings, ρ is the pyroelectric coefficient for the transducer, Q is the Q of the transducer, and ω_o is the first resonance of the PZT.

Numerical Results. We consider a numerical example. For our PZT, $C = 1.2 \times 10^{-8}$ F, $A = 1 \times 10^{-5}$ m^2, $\tan\delta = 0.01$, $L = 1.78 \times 10^{-4}$ m, $\sigma = 10^{-11}\ \Omega^{-1}$ cm^{-1}, $g_H = 7.019 \times 10^2$ J/sec/°C, $\rho = 0.1 \times 10$ coul/cm^2/°C, $\rho_o = 5.2$ g/cm^3, $C_v = 0.4$ J/g/°C, $Q = 75$, $\omega_o = 2\pi(5 \times 10^5)$. Using the noise figures for our lock-in amplifier we get the noise shown in Table 1. The measured system noise was 17 nV/Hz$^{1/2}$ at 16.6 Hz for a totally isolated detector. The agreement between the theoretical and measured noise is fortuitous since many factors such as $\tan\delta$ are estimates. However, these values are useful for assessing the relative contributions of the different noise sources.

The measured voltage responsivity was giving an $NEP_V = 5 \times 10^{-8}$ W at 16.6 Hz. If the dielectric loss tangent does not become significantly large at lower frequencies, operation at 5 Hz can improve this figure somewhat. In our experiments, we achieved an NEP of 1×10^{-7} W for thin metals and 6×10^{-7} W for transparent samples.

Discussion

Despite the complex nature of the problem, we have shown that our three-dimensional treatment

Table 1. Noise contributions ($nV/\sqrt{Hz}$).

Source	Magnitude ($nV/Hz^{1/2}$)
Electronic	12.9
Dielectric loss	11.42
DC leakage	0.61
Brownian motion	1.37
Thermal	1.67
Total rms	17.4

yields a simple expression (Eq. 1) which quantitatively describes the experimentally observed PZT photoacoustic signal.

We show that the PZT measures the temperature distribution within the sample. There is no complication due to the delay or propagation of a thermally induced sound wave. For thermally non-conductive samples, the temperature distribution is proportional to the heat deposited per volume.

It is important to point out that our theory is not a linearized theory, and it does not assume that the sample is thin, although in thin sample cases one can derive an identical expression using thin plate theory. Our theory is applicable for $\alpha\ell$ as high as 10 for thermally non-conductive media. The applicability of this theory may be readily extended beyond the limitations of our assumptions and without appreciably altering our findings.

Several simplifications of the theory which cannot easily be eliminated should be noted. The first one involves neglecting the interaction between the sample and the PZT. If the sample is thick compared to the PZT and the PZT is relatively compliant, the tranducer measures the strain of the sample as assumed by the theory. If, however, the transducer thickness is comparable to or larger than that of the sample, the theory may be expected to break down for three reasons. First, the transducer will measure the stress in the sample rather than the strain. Second, the expansion of the sample will be altered. Finally, the neutral surface (the surface of zero displacement) for the transducer-sample combination is located within the transducer. This causes a reduction in the signal since the piezoelectric material on one side of the neutral surface expands while it compresses on the other sides. These two contributions tend to cancel out, reducing the net signal. Consequently, although the signal to noise ratio improves as the transducer gets thicker, the theory may no longer be valid.

A second limitation concerns the contribution of the pyroelectric effect. If significant amounts of heat are transmitted to the transducer, the transducer would develop thermal stresses of its own and produce a voltage due to the pyroelectric effect. This would become significant only in the case of very low chopping frequencies, high thermal conductivities of the sample, and thermally conductive adhesive.

Finally, the transducer restricts large bending motions even if it is relatively compliant or thin compared to the sample. Hence, one expects that at high absorptions and low diffusivities the bending contribution may be somewhat less than that theoretically predicted.

From an experimental viewpoint, the main factor limiting the detector performance is the background signal which results from the scattering of light on the PZT. This background signal is wavelength dependent and can be minimized, for example, by depositing a layer of highly reflecting material on the PZT before coupling it to the sample.

Considerations for Detector Optimization and Final Remarks

Equations 5-10 do not yield an absolute value for the NEP. However, they do give the relative dependence of the NEP on various important parameters and can be used for the purpose of optimizing the PZT-PAS detector. In Table 2, we give a set of rules of thumb for an optimized detector.

In conclusion, we have presented and experimentally verified a theoretical model which quantitatively accounts for the PZT photoacoustic signal. This should enhance the utility of PZT-PAS as a useful spectroscopic tool. We have also shown that the PZT directly detects heat-induced strain caused by the absorption of electromagnetic radiation.

FOOTNOTE AND REFERENCES

*The complete version of this work was published in J. of Appl. Phys. 51, 3343 (1980).

1. L. B. Kreuzer, J. of Appl. Phys. 42, 2934 (1971).
2. J. G. Parker and J. Ritke, J. Chem. Phys. 59, 3713 (1973).
3. R. D. Kamm, J. App. Phys. 47, 3550 (1976).
4. R. Gerlach and N. M. Amer, App. Phys. Lett. 32, 228 (1978).
5. L. J. Thomas, M. Kelly, and N. M. Amer, App. Phys. Letters 32, 736 (1978).
6. D. Wake and N. M. Amer, Appl. Phys. Lett. 34, 379 (1979).
7. J. F. McClelland and R. N. Kniseley, Appl. Phys. Lett. 28, 467 (1976).
8. G. C. Wetsel, Jr. and F. A. McDonald, J. Acoust. Soc. Am. 60, S52 (1976).
9. C. K. N. Patel and A. C. Tam, Appl. Phys. Lett. 34, 760 (1979).
10. A. Rosencwaig and A. Gersho, J. Appl. Phys. 47, 64 (1976).

Table 2. Recommendations for signal to noise optimization.

Category	Quantity	Recommendation
Electronic	g_m	large
	1/f noise	small
	I_g	small
	PZT Area	small
	PZT Thickness	large[a]
	Sample Thickness	large[a]
PZT Properties	e_{31}^P	large
	$\tan\delta$	small
	ε_{33}^P	small
	σ	small
	ρ	small
Sample Properties	a_t	large
	$(\rho C)_{sample}$	small
	T_{PZT}	low
Modulation Frequency	ω	low[b]

[a]The sample should not be much thinner than the PZT, otherwise the neutral surface of the PZT-sample configuration will occur within the PZT leading to a reduction of the signal.

[b]The amplifier voltage NEP goes down as the frequency until the amplifier current noise NEP dominates. Further reduction will not improve the signal to noise ratio because of the difficulty in isolation low frequency vibrations.

11. L. C. Amodt, J. C. Murphy and J. G. Parker, J. Appl. Phys. 48, 927 (1977).

12. H. S. Bennett and R. A. Forman, Appl. Optics 15, 1313 (1976).

13. H. S. Bennett and R. A. Forman, J. App. Phys. 48, 1432 (1977).

14. J. G. Parker, Appl. Optics 12, 2974 (1973).

15. S. A. Schleusener, J. D. Lindberg, K. O. White, and R. L. Johnson, Appl. Opt. 15, 2546 (1976).

16. Z. Yasa, N. M. Amer, H. Rosen, A. D. Hanson, and T. Novakov, Appl. Optics 18, 2528 (1979).

17. Eastman 910 is a cynoacrylate adhesive manufactured by Eastman Company.

18. TRA-CON 2113 low viscosity epoxy manufactured by TRA-CON.

19. A. Van der Ziel, Noise in Measurements (John Wiley and Sons, New York, 1976).

20. C. B. Roundy and R. I. Byer, J. Appl. Phys. 44, 929 (1973).

A New Method for the Determination of Absolute Absorption Coefficients by Photoacoustic Spectroscopy

It has been well recognized that photoacoustic spectroscopy provides a sensitive means for measuring absorption coefficients (α) of various substances. One method for the determination of α is a least square fit of the data as a function of frequency using the general expression for the photoacoustic signal.[1] Another approach is to obtain a reference signal from a medium with identical thermal properties to that of the sample of interest but with a different yet known absorption coefficient.[2] By taking the ratio of the two signals, unknown constants other than the absorption coefficients cancel and α is thus determined. However, for many substances (particularly solids) such a reference is not readily available.

We describe here a novel approach which uses the sample itself to yield the reference signal (Fig. 9). We show that for high frequency modulation at which the sample is thermally thick, the ratio of signals S_2 and S_1 (obtained when the light is incident on W_2 and W_1, respectively) yields a measure of α as given by $S_2/S_1 = k \exp(-\alpha\ell)$ where k is a correction factor for reflection at the boundaries.

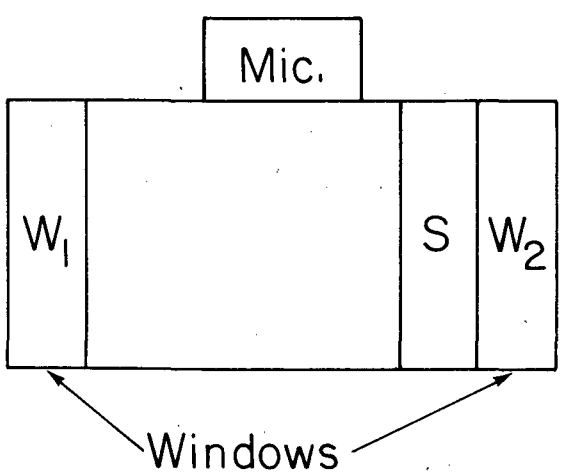

Fig. 9. Experimental apparatus. (XBL 8010-4443)

REFERENCES

1. G. C. Wetsel, Jr. and F. A. McDonald, Appl. Phys. Letters 30, 252 (1977).

2. A. C. Tam, C. K. N. Patel, and R. J. Kerl, Opt. Letters 4, 81 (1979).

A Novel Approach to Photoacoustic Determination of the Thermal Diffusivity of Condensed Matter

We report on a new method for determining the thermal diffusivity of liquids and solids.

Consider the experimental geometry shown in Fig. 10. For a highly absorbing sample M, the ratio of the magnitudes of the signal (S_2) obtained when the beam is incident from the sample side to that obtained when it is incident on the window side (S_1) gives a measure of the thermal diffusivity as shown below:

$$S_2/S_1 = \left\{\cosh^2 (\pi f/\beta)^{1/2}\ell - \sin^2 (\pi f/\beta)^{1/2}\ell\right\}^{-1/2}$$

where β is the thermal diffusivity, f is the modulation frequency, and ℓ is the sample thickness.

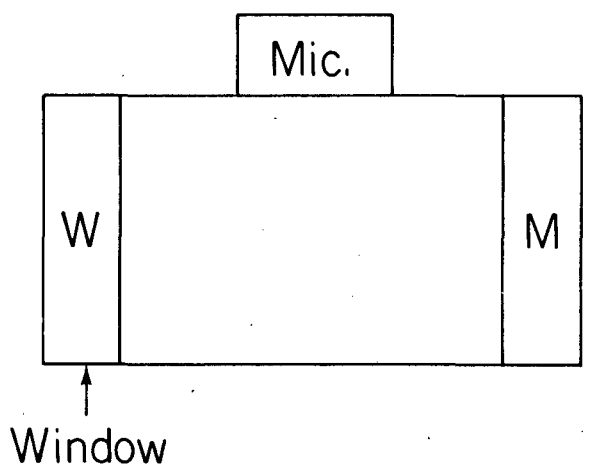

Fig. 10. Experimental apparatus. (XBL 8010-4442)

A Photoacoustic Investigation of Urban Aerosol Particles*†

The nature of the absorbing species in atmospheric aerosol particles has recently attracted considerable attention among atmospheric and environmental scientists. Recent studies using Raman spectroscopy and an optical attenuation technique[1] indicate that the absorbing species in urban particulates is "graphitic" carbon. We report here on the results of a photoacoustic investigation which gives an independent verification of the hypothesis.

Unlike conventional optical absorption techniques, photoacoustic spectroscopy measures the energy deposited in a sample due to absorption.

Since questions have been raised whether the optical attenuation technique exclusively measures the absorbing rather than the scattering component of the aerosol, a comparison between photoacoustic and optical attenuation measurements made on the same aerosol sample should help resolve this ambiguity.

The photoacoustic measurements were made in an acoustically nonresonant detector with cylindrical geometry (Fig. 11). A Knowles microphone (Model BT-1759) was used, and the cell dimensions were 2.1 cm in diameter and 0.3 cm in length. The gas in the detector cell was air at atmospheric pressure. A He-Ne laser operating at 632.8 nm with 0.5 mW of power was used as the light source, and the experiments were performed at a modulation frequency of 20 Hz. The aerosol particles, collected on 1.2-μ Millipore filter substrates, were mounted on a 1.5-mm-thick Pyrex backing with the particles facing the incident light beam. Experiments were also performed with the laser beam first incident on the filter substrate.

In the limit of low frequency light modulation ($\leqslant 100$ Hz), it can be shown[2,3] that the photoacoustic signal is given by:

$$V(\omega) = \frac{\eta\gamma PW\mu_g\mu_{sb}G(\omega)}{2\sqrt{2bkTVK_{sb}}}\left[1-\exp(-\alpha\ell)\right] \qquad (1)$$

where

- η - heat conversion efficiency
- γ - specific heat ratio for air (C_p/C_v)
- P - cell pressure
- W - input power
- μ_g - thermal diffusion length in air
- μ_{sb} - thermal diffusion length in substrate
- $G(\omega)$ - microphone response
- b - dimensionless parameter taking into account the diffusion of heat from the sample to the Pyrex backing
- T - temperature
- V - cell volume
- K_{sb} - thermal conductivity of substrate
- α - absorption coefficient
- ℓ - effective path length.

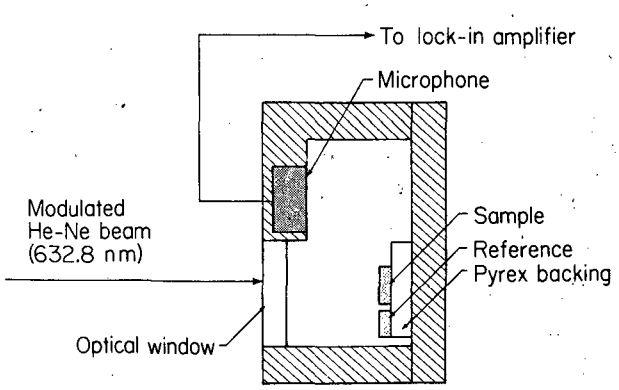

Fig. 11. Experimental arrangement. (XBL 794-1230)

From Eq. (1) it follows that the photoacoustic signal saturates exponentially with increasing absorption to a value of

$$V_{sat}(\omega) = \frac{\eta\gamma PW\mu_g\mu_{sb}G(\omega)}{2\sqrt{2bTVK_{sb}}} . \qquad (2)$$

Hence the ratio of the signal from a given sample to a reference sample for which the signal is saturated yields

$$S_{ph} = V/V_{sat} = 1-\exp(-\alpha\ell) . \qquad (3)$$

This saturable behavior was observed for highly absorbing samples, and the sample which yielded the largest photoacoustic signal was used as the reference, V_{sat}. Note that such samples yield values of $\alpha\ell \geqslant 3$, as deduced from the optical attenuation measurements; hence the highest signal obtained from available samples is close to the actual saturation value.

The experimental setup for the optical attenuation measurements is described elsewhere.[1] In this technique the signal S_{op} is defined as $1-\exp(-x)$. x is the optical attenuation of the sample and is given by $-\ln I/I_0$, where I is the transmitted intensity of a loaded filter, and I_0 is the transmitted intensity of a blank filter.

In Fig. 12 we present a plot of the normalized photoacoustic signal S_{ph} vs. S_{op} for a wide range of ambient samples and samples collected directly from combustion sources. The samples include urban particulates collected over a 24 hour period in Fremont and Anaheim, California; Denver, Colorado; and New York, New York; and particles collected in a highway tunnel and from an acetylene torch. The least squares fit of the experimental points yields a correlation coefficient r of 0.98 and a slope of 1.03, which would be expected if both techniques measure the same optical property of the aerosol particles. Since the photoacoustic signal is proportional to the heat generated by absorption, we conclude that the optical attenuation method measures the light absorbing component of the aerosol particles.

From a theoretical point of view, this result is somewhat surprising since aerosol particles have a large scattering coefficient, which would be expected to contribute to the optical attenuation measurement and not to the photoacoustic signal.

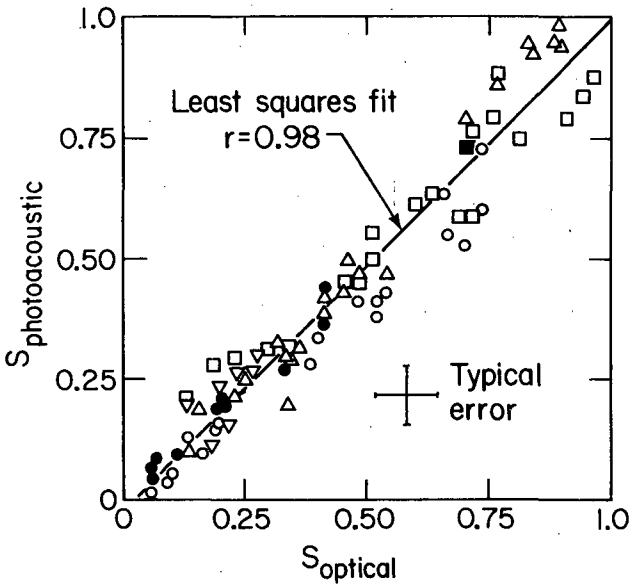

Fig. 12. Plot of S_{ph} vs. S_{op} for various samples: ▽ - Fremont; - Anaheim; ○ - Denver ▲ - New York City; ■ - highway tunnel; ● - acetylene torch. The solid line is a least squares fit of the data. (XBL 794-1229)

However, careful examination of the experimental arrangement shows that the incident light interacts not only with the aerosol particles but also with the filter medium, which is almost a perfect diffuse reflector. In this circumstance, it is possible to show[4] that because of multiple reflections between the particles and the filter substrate, the optical attenuation measurement is insensitive to the scattering properties of the aerosol.

In conclusion, the results presented here, when combined with Raman scattering data[1] and thermal analysis[5] and solvent extraction results,[6] indicate that the optically absorbing component of urban aerosol particles is "graphitic" carbon.

FOOTNOTES AND REFERENCES

*Appeared in Applied Optics, 18, 2528 (1979).

†In collaboration with H. Rosen, A. D. A. Hansen and T. Novakov of the Atmospheric Aerosol Research Group at LBL.

1. H. Rosen, A. D. A. Hansen, L. Gundel, and T. Novakov, "Identification of the optically absorbing component in urban aerosols," Appl. Opt. 17, 3859 (1978).

2. Over a frequency range of 5-100 Hz, the photoacoustic signal showed no variation, indicating that the sample was thermally thin. In this case, Eq. (1) follows from Eq. (21) of Ref. 3 in the limit of $\omega \to 0$ and after modification of their parameter b to take into account an additional boundary layer introduced by the Millipore filter.

3. A. Rosencwaig and A. Gersho, "Theory of photoacoustic effect with solids," J. Appl. Phys. 47, 64 (1976).

4. H. Rosen and T. Novakov, "Optical attenuation: a measurement of the absorbing properties of aerosol particles," in Atmospheric Aerosol Research Annual Report 1977-78, Lawrence Berkeley Laboratory Report LBL-8696, p. 54.

5. H. Rosen, A. D. A. Hansen, L. Gundel, and T. Novakov, "Identification of the graphitic carbon component of source and ambient particulates by Raman spectroscopy and an optical attenuation technique," Proceedings, Conference on Carbonaceous Particles in the Atmosphere, Lawrence Berkeley Laboratory, 1978 (in press).

6. R. E. Weiss, A. P. Waggoner, R. J. Charlson, D. L. Thorsell, J. S. Hall, and L. A. Riley, "Studies of the optical, physical, and chemical properties of light absorbing aerosols," Proceedings, Conference on Carbonaceous Particles in the Atmosphere, Lawrence Berkeley Laboratory, 1978 (in press).

Photoacoustic Characterization of the Optical Properties of Hydrogenated Amorphous Silicon

Recently, there has been strong interest in amorphous silicon and hydrogenated amorphous silicon because of their potential photovoltaic applications and their unique properties as amorphous materials.

The amorphous silicon hydrogen films (a-Si:iH) are produced either by r.f. decomposition of silane (SiH_4) or sputtering silicon targets in a hydrogen environment. The resulting films can contain up to 50 atomic percent hydrogen which gives the films their interesting properties. The films have an optical band gap which varies with hydrogen content from 1.2 ev to 2 ev and, unlike other amorphous materials, can be both n and p-type doped. The latter property allows one to construct solar cells from a-Si:iH films which could be manufactured for much lower cost than current crystalline solar cells.

The role of hydrogen in determining the density of states in the gap, defect traps, recombination centers, and doping mechanisms are poorly understood at present. The usual method of studying such problems is to measure the absorption of the sample using radiation of energy less than the band gap. Since the thin films have weak absorption and scatter significantly, conventional absorption measurements yield inaccurate or misleading results.

We have developed a sensitive photoacoustic technique which solves these problems. Since the technique only measures the power absorbed, we find that it is very sensitive to small absorption and is insensitive to scattering.

Using a dye laser, we have obtained spectra over limited regions of the visible which are quite similar to traditional absorption measurements.

We are extending our measurements to 1 μ (1.2 ev) by using appropriate dyes.

Due to the greater tuning range of pulsed laser sources in the 1-2.2 μm region, we are currently investigating the pulsed response of our photoacoustic signal. The integral of the peak response of the detector over short time periods after the laser pulse arteries can be related to the absorption of the sample. Consequently, we should be able to extend absorption measurements throughout the region below the band gap of 1.5 ev.

Having demonstrated the feasibility and power of our photoacoustic technique, we plan to make systematic measurements of the gap absorption as a function of film quality, hydrogen content, defect, and impurity concentration, and doping levels. Such measurements enable us to understand those factors which determine the ultimate conversion efficiency of amorphous photovoltaic devices, and will shed light on some aspects of the physics of amorphous semiconductors.

APPLICATIONS OF LIQUID CRYSTALS

The liquid-crystalline state of matter is characterized by a spontaneous anisotropic order and by fluidity. The anisotropic order leads to anistropy in the physical properties of the medium, and the fluidity makes it easily susceptible to external perturbations. Such perturbations can be in the form of electric or magnetic fields, pressure or temperature. In addition, we have demonstrated that certain gaseous organic pollutants change the liquid-crystalline structure. This change, which is readily detectable, is the basis for an inexpensive and sensitive (10^6) personal dosimeter for some organic pollutants. Two other applications of liquid crystals are described below.

Liquid Crystal Magnetometer

The purpose of this program is to develop a sensitive (fraction of a gauss) and simple dosimetry technique for occupational exposures to magnetic fields in fusion plants. Our approach will involve the use of ferro-nematic and ferro-cholesteric liquid crystals.

The physics behind the proposed device is that incorporating non-spherical magnetic grains into the liquid crystal matrix allows the nematic and cholesteric molecular orientation to be coupled to a very weak external magnetic field. The coupling, which is mechanical in nature, is due to the elastic properties of the liquid-crystalline phase. This coupling is what we proposed to exploit as the basis for our magnetic dosimeter.

Specifically, the orienting effect of the "host" liquid-crystalline matrix upon the "guest" magnetic grains results in a net magnetization in the absence of an applied field, and this remnant magnetization provides the mechanism for coupling to the external magnetic field. At zero external field, the ferro-liquid crystal exhibits certain optical properties. In the case of ferro-cholesterics, a specific wavelength of light is selectively reflected. For ferro-nematics, a given light intensity is transmitted through the birefringent sample.

Upon the application of an external magnetic field (as weak as one gauss), the coupling of the spontaneous magnetization to the field induces the disruption of the liquid-crystalline order causing the optical properties of the matrix to change: (1) in the case of ferro-cholesterics the wavelength of the selectively reflected light will vary as a function of the applied field, and at a critical field strength, complete disruption of the cholesteric order will occur; (2) in the case of ferro-nematics, as the external field increases, the matrix birefringence will change and the intensity of light transmitted through crossed polarizers will vary. As in the case of ferro-cholesterics, at a certain critical external field, total disorder of the nematic phase sets in.

Typical preliminary results are shown in Fig. 13 depicting the change in induced birefringence as a function of applied magnetic field.

Fig. 13. The change in induced birefringence as a function of applied external magnetic field. (XBB 793-3173)

To prevent the magnetic grains (Fe_2O_3) from floculating, the following procedure was adopted. The magnetic grains are ellipsoidal in shape and are approximately 0.5 μ long; the aspect ratio is approximately 7:1. In addition, the particles carry a magnetic dipole moment, averaging 2×10^{-12} gauss-cm^3.

The earliest attempts to disperse the particles involved placing them directly in the liquid crystal (MBBA) at room temperature (T_r) and sonicating. It was observed that dispersion is difficult, particularly in light of the large energy associated with adjacent magnetic dipoles ($\sim 10^5 k_b T_r$). Furthermore, once the particles were dispersed, there appeared to be a strong tendency to reclump, the result of strong magnetic interactions as well as Van der Waal attractions.

To overcome these difficulties, a multistep procedure has been implemented. The magnetic particles are first placed into an approximately 10 percent (by weight) solution of hexadecyl-trimethyl-ammonium-bromide (HTAB) in chloroform. The entire mixture is placed in a bottle, along with a dozen small steel balls, and agitated in a vortex mixer for several minutes. The turbulent motion is sufficient to overcome the large dipolar energy, and the particles are readily separated. During this time, the non-polar ends of the HTAB molecules attach themselves to the magnetized particles, while the polar heads protrude into the highly polar chloroform.

The mixture is allowed to sit for about 30 minutes, during which time the largest non-dispersed aggregates settle out. A sample from the fine suspension (top) is removed and slowly centrifuged until nearly all the particles have settled out. The remaining suspension, composed of chloroform, HTAB, and well-dispersed HTAB-coated particles, is removed and again centrifuged this time at high speeds, forcing all the remaining particles to settle. The chloroform and HTAB solution on top is then poured off, and new chloroform is added. In this way the excess HTAB is disposed of.

The system of chloroform and HTAB-coated magnetic particles is again shaken in the vortex mixer to redisperse the particles. Since the head groups of the HTAB are sufficiently polar, they tend to prevent the particles from reclumping. (At this point it may be necessary to repeat the procedure, beginning with rapid centrifugation, to further dispose of any remaining excess HTAB.)

A sample of chloroform and well-dispersed HTAB-coated particles is then mixed in equal amounts with MBBA. By heating the system and simultaneously vacuum pumping, it is possible to purge nearly all the chloroform, leaving a mixture of HTAB-coated particles in a matrix of MBBA which provide the matrix for our dosimeter.

Novel Applications of Amphiphillic Liquid Crystals for Energy Production

The polymorphism of amphiphillic liquid crystals can be exploited for the recovery of oil from oil shale and for cleaning oil spills. However, the nature of such polymorphism is not well characterized. One of the goals of our research is to gain a better understanding of the behavior of these amphiphillics and to devise the optimum parameters for their utilization as a means of oil extraction.

The molecules being studied contain both polar and non-polar regions (amphiphillic molecules) and it is this property that gives the substance its interesting behavior. For example, bulk solutions containing a few percent of water exhibit a complex liquid crystalline behavior. Bilayers of such molecules have been studied as models for the cell's membrane. One can also form monomolecular films using amphiphillics and this is where our interest lies. In particular, we form a layer at the interface between water and a non-polar hydrocarbon solvent. This layer ranges in surface density from zero up to a maximum molecular density before the 2-d monolayer collapses into a more thermodynamically stable 3-d system. Within this density range, for various temperatures, we are able to measure the 2-d equivalent pressure and thus generate phase diagrams and possibly also study some nonequilibrium properties. In our recent work, we have observed phases that perhaps correspond to the 2-d equivalent of a solid, liquid, and liquid crystalline phases. Our earlier work investigated the phase transitions of these monolayers at the air/water interface using the non-perturbing technique of light scattering to probe the physics of the monolayer. We are now trying to clarify some of the many unanswered questions concerning films at the water/oil interface. These questions include the nature of the phases, whether the transitions are first or second order, the local symmetry of the "solid" region and the importance of possible three dimensional effects.

Our experimental method is to study the light scattered from thermally excited interfacial ripples or "ripplons". Thermal fluctuations of the system near room temperature spontaneously produce surface waves of a few angstroms mean amplitude. (By comparison, the lipid molecules we are studying, L-α-DPPC, are about 25 angstroms long and can be compressed to a maximum surface density of 30 square angstroms per molecule.) These ripplons move with a velocity which varies with the monolayer concentration and have a lifetime dependent on surface as well as bulk viscosities. Thus if we choose to measure only ripplons of a precise $\underline{q}$, by scattering into a lens/pinhole system at $\approx 1^\circ$, we can extract physical information by analyzing the doppler shifted laser frequency and the lifetime determined linewidth. Since frequency shifts due to ripplon-photon scattering are on the order of tens of kilohertz, we use light beating spectroscopy. The scattered, frequency-shifted beam is mixed with unshifted laser light and the two beat together on the photocathode of a PMT. Using photon counting techniques, this signal is fed to a digital autocorrelater and the resulting time domain spectrum is then fit by an in-lab computer. Thus if we know the ripplon $\underline{q}$, we are able to extract the frequencies and damping coefficient of the ripplon. Then, using hydrodynamics we extract the 2-d pressure (surface tension) and viscosity. Since we already know temperature and density (we vary density with an all glass, specially coated compression piston) we have all variables required

to study the phases of the system, thus obtaining the equilibrium thermodynamic properties of this 2-d system.

Other parameters can also be varied such as length of the molecule, type of polar and non-polar region, chain length of the hydrocarbon solvent, etc. In addition, one must be very careful about surface absorbing impurities. This puts very stringent purity requirements on all components of the system. Room vibration effects must also be minimized and a precision, actively leveled, air piston isolated optical table has been set up. Temperature control is also critical since the laser beam is totally internally reflected from the oil/water interface and convection currents tend to grossly defocus the laser beam.

Some of these experimental difficulties were overcome during the early work of H. Birecki and N. M. Amer investigating films at air/water interfaces.[1] We have subsequently developed the light scattering technique for oil/water systems and are now setting up a new experimental cell designed to eliminate problems we encountered earlier and to deal with new difficulties peculiar to liquid/liquid systems. During initial oil/water monolayer experiments, we were able to perfect the injection technique used to apply the molecules to the liquid interface. We also observed the expected change in surface density due to the oils' solvation of the lipid's tails. The elimination of what may have been a 2-d liquid-gas coexistence region in the earlier air/water interface experiments was also seen. Mutual attraction of the DPPC molecules' tails would presumably have provided the mechanism for this transition. This attraction is greatly reduced by the hydrocarbon solvent. In addition, we have paid close attention to items such as impurities, monolayer leaks, temperature gradients, and q calibration in the new cell. We anticipate clean data from this set up with the emphasis on carefully measuring the phase transitions in this 2-dimensional system. Once this is achieved, work on vesicle formation and emulsification in this amphiphillic system will be initiated.

*This work supported by DOE/EV, Office of Pollutant Characterization and Measurement.

REFERENCES

1. H. Birecki and N. Amer, Journal de Physique 40, C3-433 (1979).

2. H. Birecki and N. Amer, Bull. Am. Phys. Soc. 24, 251, A09 (1979).

FUTURE DIRECTIONS

Laser photoacoustic detection work will continue in the direction of developing ultra-sensitive multiparameter molecular detectors for the characterization of gaseous trace contaminants, particularly those associated with synfuels. We plan to extend optoacoustic detection to water pollutants, with specific emphasis on nitrates, sulphates and organic contaminants. Efforts will be given to the elemental detection and analysis by a tunable laser photoacoustic spectrometer. Our collaboration with the Atmospheric Aerosol Research Group at LBL will continue investigating optical properties of carbonaceous particulates.

Research on the optical characterization of amorphous silicon will continue to study the optical nature of the "gap states". De-excitation mechanisms of the photoexcited amorphous films will be investigated, and photoacoustic spectra of hydrofluorinated amorphous silicon will be obtained. Our prime motivation is to explore optically the means of achieving higher conversion efficiencies from these devices.

Various applications of liquid crystals will continue to be explored. Optimization and comparison of ferro-nematic and ferro-cholesteric dose-integrating magnetometers will be made, and prototypes will be constructed; the actual field tests will be conducted in magnetic fusion experimental areas. Work on gaseous organic detectors will aim at investigating the fundamental mechanism responsible for the observed effect, and sensitizers will be incorporated in the liquid crystal detector to adjust the concentration threshold. Finally, in the case of lyotropic monolayers, work will continue on the oil-water interface, and the investigation of emulsification and vesicle formation will be carried out.

OPERATION OF A GAS CHROMATOGRAPH/MASS SPECTROMETER FOR THE IDENTIFICATION OF COMPONENTS IN FOSSIL ENERGY AND ENVIRONMENTAL SAMPLES*

A. S. Newton and W. Walker

The Finnigan Model 4023 gas chromatograph/mass spectrometer/data system has operated with few problems other than routine maintenance during the year. The system has been operated almost exclusively with a 30 meter, OV-101 capillary column. This column gives excellent results with most samples, and mixtures too complex to be resolved on this column are unlikely to be better resolved on a different type column. In some cases, however, major components in a mixture will elute at identical times even with capillary column separation ability (~100,000 theoretical plates). For iden-

tification, if the compounds are of unrelated types, it is often possible to determine that an obvious mixture exists and to identify each component present. A case of this type was observed in the reconstructed ion chromatogram (RIC) of a mixture of fatty acid methyl esters contaminated in the methylation step by methylated cyclo siloxanes. The heptanoic acid methyl ester and octamethyl cyclo tetrasiloxane each eluted at 744 seconds. Each compound was identifiable in the mixture owing to the very different mass spectra of the two materials. A different type chromatographic column would have separated the two compounds.

Attempts to use the Finnigan GC/MS in the chemical ionization mode have not been successful, and work needs to be done in improving the operation in the CI mode.

During the past year the system has been used for the investigation of approximately 400 samples, including several test mixtures. Each research group submitting samples for the instrument has different type samples and the problems of investigating the samples differ. Most samples received have been complex, containing more than 20 components each. A few have hundreds of components and the reconstructed ion chromatogram is a manifold of largely unresolved gas chromatographic peaks.

It is not possible to identify every component in a complex mixture. However, for those components with well resolved chromatographic peaks and mass spectra of good quality, information on molecular weight and composition can be obtained from good parent ion intensity information. From the occurrence or non-occurrence of mass peaks at key mass numbers, it is frequently possible to identify the component as a compound type without identification of the specific isomer present. This is particularly true of compounds containing long alkyl groups. The number of isomers possible in 8 or 9 carbon alkyl or alkenyl groups is formidable. A separate analysis of each mass spectrum by a knowledgable chemist may lead to the identification of the compound from which the spectrum was derived. This is, however, too time-consuming to be used as a general procedure unless the specific identification is of prime importance.

A very interesting series of samples resulting from the catalytic polymerization of the low molecular weight alkenes (C_2H_4, C_3H_6, and i-C_4H_8) were studied. The polymerization products were higher alkenes in the C_8 to C_{20} carbon number range. While the mass spectral libraries have the mass spectra of only a few isomers of alkenes in this molecular weight range, the interaction of the mass spectroscopist with the experimenter resulted in the identification of many specific branched alkenes from the fragmentation patterns of each chromatographic peak with some knowledge of the polymerization mechanism.

Air samples taken in Tenax sampling tubes have been studied for the identification of organic compounds in air. As the GC/MS has not yet been adapted for directly accepting the gaseous products desorbed from the Tenax collectors, the air impurities were desorbed into a small drop of pentane. The pentane solution was then investigated by GC/MS. This method has been successfully applied for the identification of many of the pollutants present in various air samples. If was found, however, that the relative amounts of each specific component in the pentane solution was highly dependent on the conditions of storage of the pentane solution before injection into the GC/MS. The ampoule cap materials were found to be selective adsorbents for trace impurities in the pentane, and even overnight storage in a refrigerator or freezer made a drastic change in the RIC of the samples. Some lighter components were completely missing after overnight storage of the sample.

Samples from the methylation of waste waters from various oil shale retorting processes have resulted in the identification of fatty acids and di-acids as significant organic contaminants of those waters. Acids from 5 to 14 carbons were identified. Branched chain fatty acids and unsaturated acids were present in lesser amounts than were the straight chain acids. A direct extract of the oil shale water shows a complicated chromatograph with some heterocyclic nitrogen bases such as the pyridines and quinolines as prominent components.

Samples of several metal-organic compounds have been investigated for their behavior in a GC/MS analysis scheme. Samples of Ni and Hg diketone complexes were not successfully chromatographed, whereas the Zn and Cu compounds were chromatographed. Much work remains to be done on various types of metal-organics before their gas chromatographic behavior can be successfully predicted and dependable identifications and analyses made by this method.

The GC/MS system has proved to be useful in many ways to other research and supporting groups at LBL. One example is the identification of chlorinated biphenyls in various transformers being replaced at LBL. This is an important problem in the disposal of these transformers.

A series of samples were studied in regard to the composition of vapors emitted from various construction materials in a vacuum. This information is of prime importance in the construction of particle detectors.

GC/MS characterization of samples derived from the extraction of sea water and of organisms living in sea water was continued. The extreme complexity of most such samples makes identification of more than a few specific components impossible. By searching the mass chromatograms of specific ions, e.g., M = 256, the possible occurrence of specific compounds can be documented, and an upper limit on the amount of such compounds present can be set within fairly wide probable error limits.

*This work was supported in part by the Assistant Secretaries of Environment and Fossil Energy, DOE.

DEVELOPMENT AND APPLICATION OF X-RAY FLUORESCENCE ANALYTICAL METHODS*

R. D. Giauque

INTRODUCTION

The development and application of trace multi-element x-ray fluorescence (XRF) analytical methods are used to support a variety of research programs. Using XRF analytical techniques, oil shale, shale oils, oil shale retort waters, liquid and solid industrial wastes, atmospheric aerosols, coal fly-ash, geological specimens, salts, foods, and alloys have been analyzed during the past year.

ACCOMPLISHMENTS DURING 1979

Members of the Instrument Techniques Group completed modifications to one of our x-ray systems. A pulsed x-ray tube was installed and the automatic sample handling system was redesigned. Subsequently, we developed computer programs applicable for analysis of both liquid and solid samples using this x-ray system. Additionally, a straight-forward procedure was established for the determination of 42 elements (Ti → La, Hg, Pb, Bi, Th, and U) in aqueous samples. Seven 4 λ droplets are placed in a reproducible geometrical array over a 1 cm^2 area on 1/4 mil polypropylene film and dried overnight in a desiccator. These samples are treated as infinitely thin specimens with no significant x-ray absorption for the elements determined. Using three different x-ray excitation conditions for each sample, and a total analysis time of approximately twenty minutes, typical sensitivities realized are in the 0.5 to 5 ppm range. Table 1 lists results determined for two industrial waste liquids. These results illustrate the capability of the method.

Additionally, a method for the direct determination of trace elements in light element matrices has been published.[1] This method was briefly described in the 1979 Energy and Environment Division Annual Report, pg. 288.

PLANNED ACTIVITIES FOR 1980

X-ray fluorescence analytical methods will be applied to support oil shale, geochemical, industrial waste management, and atmospheric aerosol research programs. A method for the determination of 42 elements in small quantities (25 mg) of geochemical samples is being developed. Additionally, a procedure for the determination of the elements Mo → Ba in oil samples will be established.

*This work supported by DOE, Basic Energy Science.

Table 1. Elemental concentrations in two industrial waste liquid samples (μg/g±2σ).

Element	HML-614	HML-615
Ti	<6	<12
V	<4	<8
Cr	88.9 ± 8.8	80.5 ± 8.0
Mn	3.2 ± 2.4	48.6 ± 5.4
Fe	379 ± 37	3920 ± 390
Co	<9	<14
Ni	1.9 ± 0.6	7.2 ± 1.4
Cu	2.8 ± 0.8	25.3 ± 2.5
Zn	48.9 ± 4.8	224 ± 22
Ga	<2	<2
Ge	<1	<1
As	<5	<5
Se	<1	<0.6
Br	<0.6	0.8 ± 0.4
Rb	<0.6	2.1 ± 0.4
Sr	2.4 ± 0.4	11.0 ± 1.0
Y	<2	2.5 ± 1.0
Zr	<0.6	9.6 ± 1.0
Nb	<0.6	<0.6
Mo	13.2 ± 1.3	1.8 ± 0.6
Ru	<2	<2
Rh	<2	<2
Pd	<2	<2
Ag	<2	<2
Cd	<2	4.8 ± 1.8
In	<2	<2
Sn	26.3 ± 2.6	86.8 ± 8.6
Sb	<3	<3
Te	<3	<3
I	<4	<5
Cs	<5	<5
Ba	36.9 ± 4.8	293 ± 29
La	<8	<8
Hf	<12	<15
Ta	<15	<22
W	<8	<15
Hg	<6	<6
Pb	312 ± 31	238 ± 23
Bi	<4	<4
Th	<3	<6
U	<5	<4

REFERENCE

1. R. D. Giauque, R. B. Garrett, and L. Y. Goda, Anal. Chem. 51, 511 (1979).

THE SURVEY OF INSTRUMENTATION FOR ENVIRONMENTAL MONITORING*

M. S. Quinby-Hunt, Y. C. Agrawal, C. R. Chen, R. D. McLaughlin, G. Morton, D. L. Murphy, and A. V. Nero

INTRODUCTION

The survey of Instrumentation for Environmental Monitoring began at LBL in 1971 and has continued to the present.[1] It has become an important resource for those involved in monitoring our environment and with controlling the emission of pollutants in various industrial processes. An analysis of the 4000 purchasers of the survey indicates that the majority of them are responsible directly or indirectly for the monitoring or control of pollutant emissions. This is an area of growing concern so that interest in the survey can be expected to increase.

The survey volumes describe the various substances, both conventional and radioactive, which may pollute the air and water surrounding us, giving their characteristics, sources and effects.[2] The methods for detecting and analyzing each pollutant are also described and compared. And finally, detailed specifications for instruments which are commerically available for carrying out the more common techniques used in each field are given in complete sets of Instrument Notes. The contents of the volumes are given in Fig. 1.

Volume 1 AIR		Volume 2 & 2A WATER	Volume 3 RADIATION	Volume 4 BIOMEDICAL
Parts 1 & 1A	Part 2			
Gases	Particulates	Calibration	Type of radiation	Gases
Calibration	Systems	Metals	Alpha radiation	CO
SO_2	Mass	Nitrogen	Beta radiation	SO_2
NO and NO_2	Size	Phosphorus	X and gamma radiation	Organics
Oxidants	Opacity	Sulfur	Neutron	Particulates
CO	Composition	Biochemical oxygen demand	Spectroscopy	Asbestos
Hydrocarbons	Mercury	Chemical oxygen demand	Personnel dosimetry	Metals
	Asbestos	Dissolved oxygen	Radionuclides	Arsenic
	Beryllium	Total organic carbon	Tritium	Beryllium
	Lead	Pesticides	Krypton-85	Cadmium
	Noise	Phenolics	Strontium-89,90	Lead
		Petrochemicals	Iodine-129,131	Mercury
		Oil and grease	Radon-222 & daughters	Nickel
		pH	Radium	Radiation
		Turbidity	Plutonium	
		Temperature	Sources	
		Radiation	Nuclear reactors	
			Mining & milling	
			Natural radiation	
			Fallout	
INSTRUMENT COMPARISONS are contained in appropriate sections				

Fig. 1. Contents of the volumes comprising the Survey of Instrumentation for Environmental Monitoring.

*This work supported by DOE/EV, Office of Health & Environmental Research.

ACCOMPLISHMENTS DURING 1979

In 1979, a number of major updates were completed. Several other updates and revisions were started. The competed updates include:

1. The Introduction for the WATER volume was revised to include an extensive discussion of Federal water regulations (including P.L. 92-500 and current changes in it).

2. The section on Metals in Water in the same volume was revised and expanded to include instrument notes on plasma emission spectrometers and discussions on atomic spectroscopy, ultraviolet spectrometry, x-ray fluorescence and neutron activation analysis.

3. Several new sections on metals were added to the BIO volume.

4. The BIO volume was expanded to include a section on Gaseous Organic Pollutants.

PLANNED ACTIVITIES FOR 1980

In 1980, several major revisions are planned. By mid-1980, the work now underway on the complete revision of the RADIATION volume will be finished. This work will include sections on Radiation Types, Monitoring by Radiation Type, and Monitoring by Radionuclide. There will be new sections on nuclear reactors, fuel processing and reprocessing. The discussion of biological effects of radiation will be brought up to date and expanded.

Further updating of the WATER volume will include sections on the halogens and cyanide, suspended and dissolved solids, asbestos and coliform bacteria.

Updates of the AIR volume, part 2, will discuss sampling and calibration, and will contain updated instrument notes on Mass and Size. Particle composition will be examined next. Some of the analytical techniques described in this section will include expanded sections on x-ray fluorescence, and new sections on techniques such as ESCA, SSMS and others.

In carrying out these revisions and updates, material is included in response to reader-expressed interest and in response to the need for consideration of pollutants associated with developing energy technologies. Much of the material in the survey has a direct bearing on the pollution problems associated with energy generation and interest in the survey can be expected to grow as the demand for new energy sources within a safe environment becomes more urgent.

REFERENCES

1. Environmental Instrumentation Survey Group, Instrumentation for Environmental Monitoring, Lawrence Berkeley Laboratory Report, LBL-1 (1971-present).

2. The report is divided into four volumes, currently in seven looseleaf binders: AIR, Part 1, Gases (2 binders) and Part 2, Particulates; WATER (2 binders); RADIATION; BIOMEDICAL.

EXTRATERRESTRIAL CAUSE FOR THE CRETACEOUS-TERTIARY EXTINCTION: EXPERIMENT AND THEORY

L. W. Alvarez,† W. Alvarez,†† F. Asaro,* and H. V. Michel**

INTRODUCTION

Abundant fossil remains provide a record of organic evolution for the last 570 million years of Earth history. During this time there have been six great biological crises, during which many groups of organisms died out. Numerous crises of less severity are also recorded.

The most recent of the great extinctions is used to define the boundary between the Cretaceous and Tertiary Periods, about 65 million years ago. At this time, the marine reptiles, the flying reptiles, and both orders of dinosaurs died out.[1] Extinctions occurred at various taxonomic levels among the marine invertebrates, for example, the ammonoid and belemnoid cephalopods and various groups of gastropods, pelecypods, brachiopods, and echinoderms. Dramatic extinctions occurred among the microscopic floating animals and plants; both the calcareous planktonic foraminifera and the calcareous nannoplankton were nearly exterminated, with only a few species surviving the crisis. On the other hand, some groups were little affected, including the land plants, crocodiles, snakes, birds, mammals, and many kinds of invertebrates.

Many hypotheses have been proposed to explain the Cretaceous-Tertiary extinctions,[2] and two recent meetings on the topic[3,4] produced no sign of a consensus. Suggested causes include gradual or rapid changes in oceanographic, atmospheric, or climatic conditions[5] resulting either from a random[6] or a cyclical[7] coincidence of causative factors, the effect of a magnetic reversal[8] or a nearby supernova.[9] Various mechanisms specific to a single group, such as disease or destruction of dinosaur eggs by mammals, are incapable of explaining why the extinctions affected many groups.

A major obstacle to determining the cause of the extinction is that virtually all available information on events at the time of the crisis deals with biological changes seen in the paleontological record, and is thus inherently indirect. Little physical evidence is available, and it, also, is indirect. This includes variations in stable oxygen and carbon isotopic ratios across the boundary in pelagic sediments, which may reflect changes in temperature, salinity, oxygenation, and organic productivity of the ocean water, and these variations are not easy to interpret.[10] These isotopic changes are not particularly striking, and taken by themselves they would not suggest a dramatic crisis. Changes in minor and trace element levels at the Cretaceous-Tertiary boundary have been noted from limestone sections in Denmark and Italy,[11] but these data also present interpretational difficulties. It is noteworthy that in pelagic marine sequences, where nearly continuous deposition is to be expected, the Cretaceous-Tertiary boundary is almost invariably marked by a hiatus.[12] Because of the lack of clear evidence outside the field of paleontology, it is still possible to argue that the various extinctions were not exactly synchronous, that they were produced by a fortuitous combination of ordinary environmental stresses, and that there really was no Cretaceous-Tertiary boundary crisis.[6]

ACCOMPLISHMENTS DURING 1979

In this work direct physical evidence was found for an unusual event at exactly the time of the extinctions in the planktonic realm. None of the current hypotheses adequately accounts for this evidence, but we have developed a new hypothesis that appears to offer a satisfactory explanation for nearly all the available paleontological and physical evidence.

Anomalous concentrations of platinum-group elements in deep-sea sediments are used as indicators of influxes of extraterrestrial material; the technique is based on the extreme depletion of these elements in the earth's crust. We have made measurements by neutron activation analysis of many elements including the platinum-group element iridium (Ir) in Upper Cretaceous-Lower Tertiary marine limestones from two areas. The first area is in the Umbrian Apennines of Italy, where recent paleomagnetic studies have established the timing of the planktonic extinction in the sequence of geomagnetic polarity reversals.[13] Analysis of the acid-insoluble clay fraction of the limestone shows iridium levels of about 0.3 ppb in the uppermost Cretaceous. The Cretaceous-Tertiary boundary is marked by a 1 cm clay layer in which iridium suddenly jumps to about an average of 6 ppb in the acid-insoluble residue, then gradually decreases to the previous background level in less than 1 m above the boundary as shown in Fig. 1. To test whether this is a local phenomenon, we have

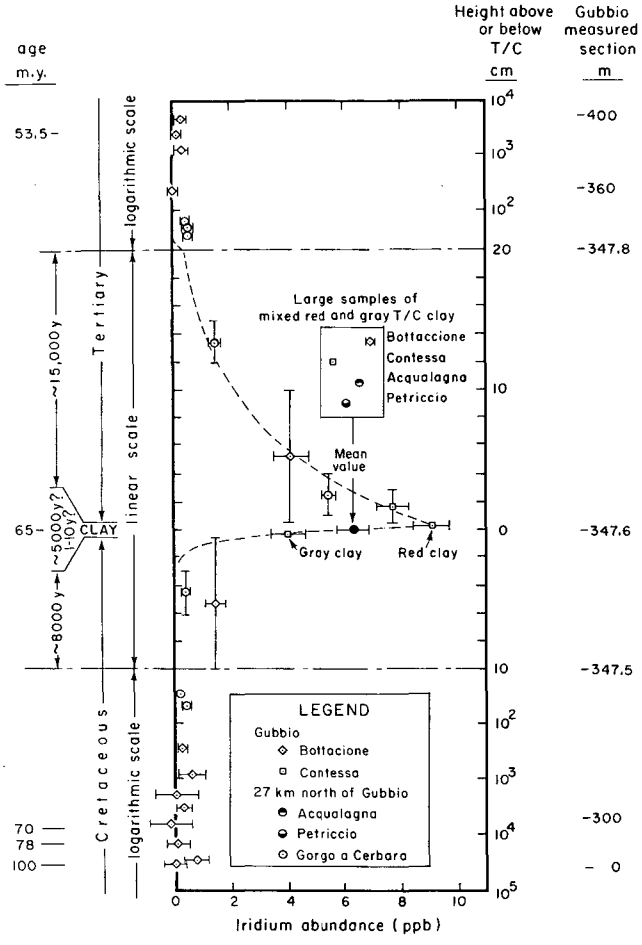

Fig. 1. Stratigraphic section at Gubbio (6,7). (a) Meter levels. (b) Systems. (c) Stages. (d) Magnetic polarity zones (black is normal, white is reversed polarity; letters give Gubbio polarity zonation, numbers are equivalent marine magnetic anomalies). (e) Lithology. (f) Samples used in first neutron activation analysis study (samples I, J, L are from equivalent positions in the Contessa section, 2 km to the northwest). (g) Formation names. (XBL 7911-13250)

analyzed samples from a classic exposure of the Cretaceous-Tertiary boundary near Copenhagen and found iridium levels nearly ten times higher than are seen in the Italian sections, with an increase from the background levels by about a factor of 160. Figure 2 shows the elemental abundances in twelve samples from Gubbio, Italy.

Discussion of these results leads to the conclusion that the anomalous iridium was probably introduced into the Earth's atmosphere as part of an abnormal influx of extraterrestrial material at the time of the extinctions. One possible extraterrestrial cause of the extinctions, a nearby supernova, has been debated for some time. Three lines of evidence are used for rejecting the supernova hypothesis:

- ^{244}Pu (80 x 10^6 yr half life) should be detectable along with Ir in the boundary clay if a supernova is responsible for the Ir anomaly, but if present, ^{244}Pu is at least a factor of 10 below predicted levels. This fact alone is not conclusive, as oceanic chemistry could alter the Ir/Pu ratio.

- The ratio ^{191}Ir/^{193}Ir might well be significantly different in supernova material at the boundary and in normal terrestrial material, but no difference was found.

- To account for the Ir seen in the boundary clay, a hypothetical supernova would have to be so close that the probability of such an event becomes vanishingly small.

We conclude that the extraterrestrial material introduced at the time of the extinctions came from a solar system source and not a galactic source (including a supernova).

After consideration and rejection of a number of possible explanations for the extraterrestrial material and the extinctions, we have developed the following hypothesis, which seems to account for most or all of the relevant observations: A number of asteriods have orbits with perihelions inside the Earth's orbit; these are called "Apollo Objects." Collisions of Apollo objects with the Earth are inevitable, and the many known meteor craters are the result. We suggest that the impact of a large Apollo object was the cause of the Cretaceous-Tertiary extinctions. Four independent calculations indicate that the impacting Apollo object had a diameter of approximately 10 km. Such an impact would produce a crater approximately 175 km in diameter. The material expelled from the crater would weigh about 100 times as much as the asteroid, and much of the combined mass would stay aloft for several years as dust in the stratosphere. Comparisons of this effect with the much smaller explosion of Krakatoa in 1883 indicate that the atmosphere would become opaque to visible light until the dust settled, although enough heat would reach the surface to prevent a major drop in temperature.

The resulting suppression of photosynthesis appears to be capable of explaining the major features of the extinctions. The marine phytoplankton would die out through loss of light with which to carry on photosynthesis. This would cause the collapse of the food chain supporting the planktonic foraminifera and the large open marine fauna, including ammonites, belemnites, and marine reptiles. Terrestrial plants would cease to grow, but would not die out because their seeds could lie dormant until the dust settled and light returned. Small terrestrial animals including the mammals, as well as the birds, would survive on a food chain based on seeds and nuts. The herbivorous dinosaurs and the carnivorous dinosaurs that preyed on them depended on a food chain based on growing vegetation; this chain would have collapsed. The survival of many marine invertebrates and aquatic animals such as crocodiles may be due to their ability to utilize food chains based on nutrients derived from decaying land plants carried by rivers to the shallow seas.

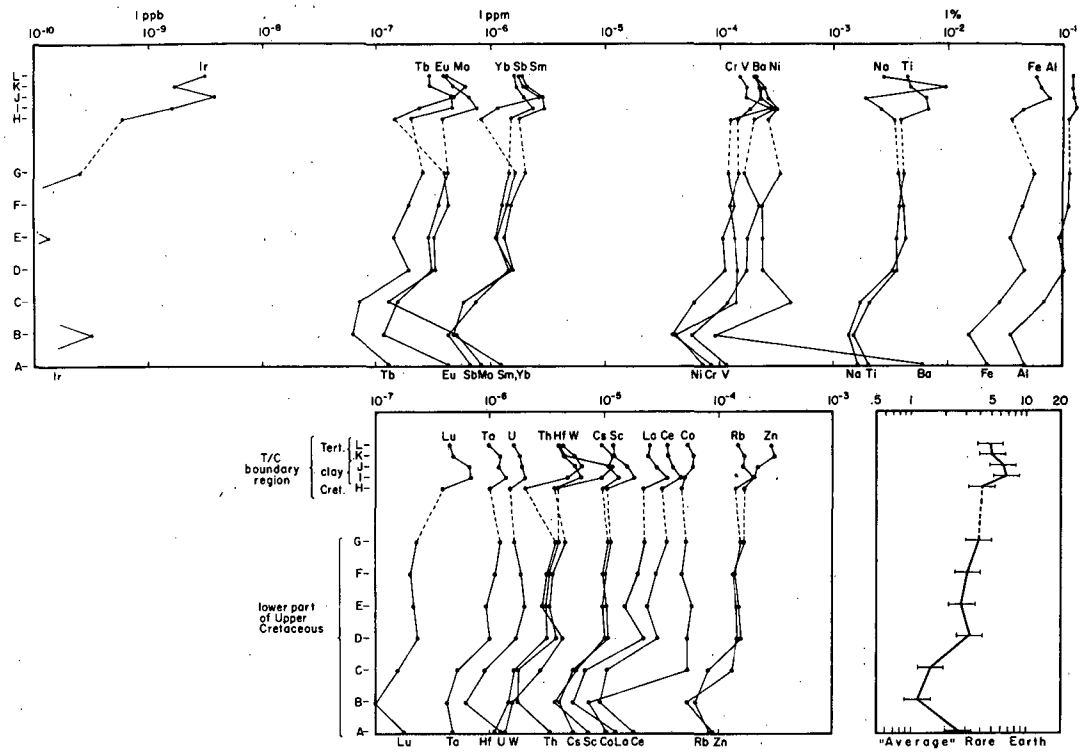

Fig. 2. Abundance variations of 28 elements in 12 samples from two Gubbio sections. (XBL 795-9861)

Thus it appears that a highly probable sequence of events could produce the observed extinctions, and independent physical evidence for this mechanism has now been found.

IDENTIFICATION OF EXTRA-TERRESTRIAL PLATINUM METALS IN DEEP-SEA SEDIMENTS

This study began with the realization that platinum group metals and some related elements (Pt, Ir, Os, Rh) are 10^3 - 10^4 times more abundant in chondritic meteorites than they are in the earth's crust and upper mantle.[14] Carbonaceous chondrites are thought to come from undifferentiated bodies giving a close approximation to average solar system elemental abundance. Depletion of the platinum group metals in the earth's crust and upper mantle is probably the result of concentration of these elements in the earth's core.

Platinum elements are apparently below detection levels in most sedimentary rocks, judging from the few published data.[15] This is reasonable because in addition to their scarcity in rocks from which sediments are derived, they are also extremely insoluble and should be present only at very low levels in river and sea water (again, data are not available).

These considerations suggested to us that much of the iridium to be found in sedimentary rocks comes from ablated meteoritic dust, deposited at a roughly constant rate. We suspected that measurement of platinum metals might shed light on the time interval represented by the 1 cm thick clay layer that marks the Cretaceous-Tertiary boundary in the Umbrian Apennines. We therefore undertook an investigation of the abundance of iridium, which can easily be determined at low limits by neutron activation analysis (NAA) because of its large capture cross section for slow neutrons, and because the gamma rays given off during de-excitation of the decay product are not masked by other gamma rays. The other platinum group elements are more difficult to determine by NAA.

After we had begun our work, we learned that this method of identifying extraterrestrial material had been suggested in the early 1950's by Pettersson and Rotschi and by Goldschmidt[16] and actually carried out in the 1960's by Barker and Anders.[17] Subsequently the method was used by Ganapathy et al.[14] to demonstrate an extraterrestrial origin for silicate spherules in deep-sea sediments. Sarna-Wojcicki et al.[18] suggested that meteoritic dust accumulation in soil layers might enhance the abundance of iridium sufficiently to permit its use as a dating tool.

We have found that iridium <u>does</u> show anomalously high abundances at exactly the stratigraphic position of the Cretaceous-Tertiary boundary in two areas, Italy and Denmark, where marine limestones preserve a complete or nearly complete record of this time interval.

ACKNOWLEDGMENTS

It will be obvious to anyone reading this paper that we have benefited enormously from our conversations and correspondence with many friends and colleagues throughout the scientific community. We would particularly like to acknowledge the help we have received from James R. Arnold, Andrew Buffington, I. S. E. Carmichael, Garniss Curtis, Philippe Eberhard, Earl K. Hyde, Christopher McKee, Maynard C. Michel (who was responsible for the mass spectrometric measurements), John Neil, Bernard M. Oliver, Charles Orth, Barrie Pardoe, and Andrew M. Sessler. One of us (W. A.) thanks the U.S. National Science Foundation for support, the other three authors thank the U.S. Department of Energy for support, and one of us (L.W.A.) thanks NASA for support. The XRF measurements of trace elements, Fe and Ti by Robert D. Giauque and the XRF measurements of major elements by Steve Flexer and Marian Sturz were most appreciated. We appreciate the assistance of Dan Jackson and Cecilia Nguyen in the sample preparation procedures. We are grateful to Tek Lim and the staff of the Berkeley Research Reactor for many neutron irradiations used in this work. We also appreciate the efforts of Gordon Pefley and the staff of the Livermore Pool Type Reactor for the irradiations used for the Ir isotopic ratio measurements.

FOOTNOTES AND REFERENCES

*Lawrence Berkeley Laboratory, University of California, Berkeley.

*†Space Sciences Laboratory, University of California, Berkeley.

††Department of Geology and Geophysics, University of California, Berkeley.

1. D. W. Russell, Geol. Assoc. Canada Sp Rep 13, 119 (1975).

2. M. B. Cita and I. Premoli Silva, Riv. Ital. Pal. Strat. Mem. 14, 193 (1974). D. A. Russell, Ann. Rev. Earth Planet. Sci. 7, 163 (1979).

3. K-TEC group. Proceedings of the Workshop held in Ottawa, Canada. 16-17, Nov. 1976. Syllogeus No. 12. Cretaceous-Tertiary Extinctions and Possible Terrestrial and Extraterrestrial Causes. Nat. Mus. of Natural Sciences.

4. T. Birkelund and R. G. Bromley, ed. Cretaceous-Tertiary Boundary Events. Symposium, Univ. of Copenhagen 1979. I. The Maastrichtian and Danian of Denmark. W. K. Christiansen and T. Birkelund ed., Symposium Univ. of Copenhagen 1979. II. Proceedings.

5. H. Tappan, Paleogeography, Palaeoclimatology, Palaeoecology 4, 187 (1968); T. R. Worsley, Nature (London) 230, 318 (1971); W. T. Holser, ibid. 267, 403 (1977); D. M. McLean, Science 200, 1060 (1978); D. M. McLean, ibid. 201, 401 (1978); S. Gartner and J. Keany, Geology 6, 708 (1978).

6. E. G. Kauffman, Ref. 4, Vol. II, p. 29 (1979).

7. A. G. Fischer, Ref. 4, Vol. II, p. 11 (1979); A. G. Fischer and M. A. Arthur, Soc. of Economic Paleontologists and Mineralogists, Sp. Pub. 25, 19 (1977).

8. J. F. Simpson, Geol. Soc. Am. Bull. 77, 197 (1966); C. G. A. Harrison and J. M. Prospero, Nature (London) 250, 563 (1974); J. D. Hays, Geol. Soc. Am. Bull. 82, 2433 (1971).

9. O. H. Schindewolf, Nenes Jahrb. Geol. Paleontol. Monatsh. 1954, 451 (1954); ibid. 1953, 270 (1958); A. R. Leoblich, Jr., and H. Tappan, Geol. Soc. Am. Bull. 75, 367 (1964); V. I. Krascvski and I. S. Shklovsky, Dokl. Adad. Nauk SSR 116, 197-199 (1957); K. D. Terry and W. H. Tucker, Science 159, 421 (1968); H. Laster, ibid. 160, 1138 (1968); W. H. Tucker and K. D. Terry, ibid. 160, 1138 (1968); D. Russell and W. H. Tucker, Nature (London) 229, 553 (1971); M. A. Ruderman, Science 184, 1079 (1974); R. C. Whitten, J. Cuzzi, W. J. Borucki, J. H. Wolfe, Nature (London) 263, 398 (1976).

10. A. Boersma and N. Schackleton, Ref. 4, Vol. II, p. 50 (1979); B. Buchardt and N. O. Jorgensen, Ref. 4, Vol. II, p. 54 (1979). L. Christensen, S. Fregerslev, A. Simonsen and J. Thiede, Bull. Geol. Soc. Denmark 22, 193 (1973).

11. N. O. Jorgensen, Ref. 4, Vol. I, p. 33 (1979). N. O. Jorgensen, Ref. 4, Vol. II, p. 62 (1979). M. Renard, Ref. 4, Vol. II, p. 70 (1979).

12. H. P. Luterbacher and I. Premoli Silva, Riv. Ital. Paleont. 70, 67 (1964); M. B. Cita and I. Premoli Silva, Riv. Ital. Paleont. Strat., Mem., 14 193 (1924).

13. M. A. Arthur and A. G. Fischer, Geol. Soc. Bull. 88, 367 (1977); I. Premoli Silva, ibid. 88, 371 (1977); W. Lowrie and W. Alvarez, ibid. 88, 374 (1977); W. M. Roggenthen and G. Napoleone, ibid. 88, 378 (1977); W. Alvarez, M. A. Arthur, A. G. Fischer, W. Lowrie, G., Napoleone, I. Premoli Silva, W. M. Roggenthen, ibid. 88, 383 (1977); W. Lowrie and W. Alvarez, Geophys. Jour. Roy. Astr. Soc. 51, 561 (1977); W. Alvarez and W. Lowrie, ibid. 55, 1 (1973).

14. R. Ganapathy, D. E. Brownlee and P. W. Hodge, Science 201, 1119 (1978).

15. J. R. DeVoe and P. D. Lafleur, Modern Trends in Activation Analysis, U.S. Government Printing Office, June 1969. J. H. Crocket in "Activation Analysis in Geochemistry and Cosmochemistry," Proc. of the NATO Advanced Study Inst., p. 339-351, Norway (1970), Universitetsforlaget 1971 OSLO.

16. H. Pettersson and H. Rotschi, Geochim. Cosmochim. Acta 2, 81 (1952); V. M. Goldschmidt, Geochemistry, Oxford Univ. Press. (1954).

17. J. L. Barker, Jr., and E. Anders, Geochimica et Cosmochimica Acta 32, 627 (1968).

18. A. M. Sarna-Wojcicki, H. R. Bowman, D. Marchand and E. Helley, private communication to F. Asaro (1975).

PRECISE ANALYSIS FOR BETTER UNDERSTANDING OF GUATEMALAN OBSIDIAN*

F. Stross, F. Asaro, and H. V. Michel

INTRODUCTION

The use of sophisticated instrument techniques has proven fruitful in the field of archaeology. Both x-ray fluorescence (XRF) and neutron activation analysis (NAA) have been applied to categorize the compositions of obsidian. During the past fifteen years, the study of the composition patterns of obsidians has been useful in establishing the course of supply routes and trade networks in Mesoamerica. A prime requirement in this work has been to provide a detailed, accurate data bank of the compositions of the regional sources of obsidian. This paper presents information on the extensive source area designated Rio Pixcayá, Department of Chimaltenango, and on recently collected material from a nearby source area, San Bartolomé Milpas Atlas, Department of Sacotepequez, the existence of which had been questioned.[1] A map of these areas is shown in Fig. 1.

RIO PIXCAYÁ

The Rio Pixcayá, Chimaltenango, source area represents a complex series of deposits. Some of the outcrops are difficult to reach, and the samples available for analysis were collected by different individuals at different times, in different geographical contexts. The region from which samples were made available lies within the triangle formed by the villages or towns of Chimaltenango, Choatalum ("Aldea Chatalun"[2]), and Comalapa, all in the Department of Chimaltenango (Fig. 1). Neutron activation analyses of samples of some of these outcrops have been recorded in an earlier report.[3] This paper presents additional information obtained by XRF as well as by NAA. The XRF results, shown in Table 1, include the ratios Rb/Zr and Sr/Zr separately, since the ratios eliminate some systematic errors of measurement. This source area is of particular interest because it was used

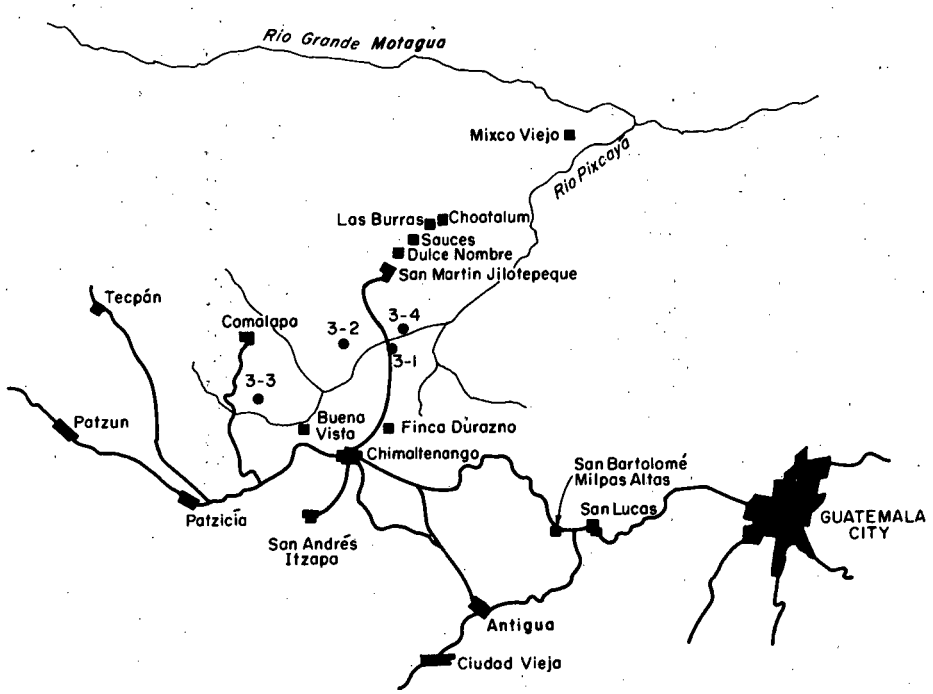

Fig. 1. Map of obsidian sources near Chimaltenango, Guatemala.

nearly 12,000 years ago,[4] although in later times it appears to have played a smaller role than the great deposits of El Chayal and Ixtepeque.

The obsidian collected from the Finca Durazno in the south[3,5] near Chimaltenango, to "Dulce Nombre" in the north, form a coherent group which probably also includes obsidian from the village Chatalun or Choatalum, somewhat further to the north. The measurements on Aldea Chatalun obsidian were made by others and cannot be directly compared with our work. Formulas were developed for comparing the different sets of data, however, and the recalibrated values for Aldea Chatalun obsidian are shown in Table 1. These are roughly consistent with the main group just discussed. Obsidian collected at "Sauces" and "Las Burras", which are reportedly located between Choatalum and San Martin Jilotepeque, are different in composition and readily distinguishable by XRF methods, as seen in Table 1.

The measurements by Zeitlin and Heimbuch[6] on "Jilotepeque" obsidian (San Martin Jilotepeque) agree most closely with the Las Burras group. The source of the "Jilotepeque" obsidian could not be ascertained from their publication.

In addition to the exploratory XRF measurements, NAA runs also were made, and they are recorded in Table 2. The samples collected in the Rio Pixcayá itself near San Martin Jilotepeque, from the Finca Durazno, and from Outcrop 3-1[1] formed a homogeneous group and are combined into a single group designated "representative Rio Pixcayá". The measurements by Hurtado de Mendoza and Jester[7] on San Martin Jilotepeque obsidian agree most closely with the Sauces group as shown in Table 2.

In summary then, nearly all source obsidian labelled Rio Pixcayá or Pixcayá appears to be of the same composition regardless of who collected or measured the obsidian. This composition pattern was found at Dulce Nombre (north of S. M. J.) as well as close to the city of Chimaltenango (Buena Vista and the Finca Durazno). Most artifacts from distant areas which have been assigned a provenience of S. M. J. or Pixcayá have this composition profile. One "source" sample collected from the Rio Pixcayá by Payson Sheets had a different profile as shown in Tables 1 and 2, and its exact geologic source is not known. Obsidian collected from S. M. J. and the region north and northeast exhibited at least two other composition patterns besides that of the Rio Pixcayá. These are shown in Tables 1 and 2 as the Sauces and Las Burras compositions.

SAN BARTOLOMÉ MILPAS ATLAS

The source area of San Bartolomé Milpas Atlas, Sacatepequez, is even less well understood than the Rio Pixcayá source. Recently, several kilograms of obsidian were collected on the Finca Nimachay (in the immediate vicinity of San Bartolomé Milpas Atlas) by the owner, Tomasa Martinez, and forwarded to us by Sr. Enrique Ruiz. Table 3 gives the detailed analyses of a sample from the Finca Nimachay.

Measurements of source material from San Bartolomé Milpas Atlas have been reported.[2,6-8] The data of Cobean and Zeitlin and Heimbuch were intercalibrated with the LBL data and agree as well as could be expected as shown in Table 3. The data of Stross et al. on many elements (not Zr) were intercalibrated with LBL data and agree as well as could be expected except for Zr. Thus, the Zr discrepancy may be a calibration problem. Intercalibration between two laboratories or sets of data does not imply one is more correct than the other, but only serves to make the data interchangeable.

The various measurements by different laboratories and techniques of obsidian from near San Bartolomé Milpas Atlas give similar abundances when intercalibrated. Thus, the source undoubtedly exists. The abundances shown for Finca Nimachay in Table 3 may be taken as representative of the San Bartolomé Milpas Atlas composition group with the qualification that the Sr and Zr values can have calibration uncertainties of ~15-20 percent.

Table 1.

Chimaltenango - Obsidian Abundances Measured by X-ray Fluorescence

					Other Composition Groups			Other Workers		
Location:	Rio Pixcayá Riverbed	Dulce Nombre	Buena Vista	Representative Rio Pixcayá	Sauces	Las Burras	Odd Sample From Rio Pixcayá Riverbed	Aldea Z & H[a] (Revised)	Chatalun Cobean[b] (Revised)	Jilotepeque[c] Z & H[a] (Revised)
No. of samples	4	5	5	14	2	5	1			
Element										
Rb	118 ± 6	115 ± 7	116 ± 6	116 ± 6	120 ± 7	106 ± 6	123 ± 6	127 ± 8	112	118 ± 11
Sr	189 ± 4	192 ± 9	188 ± 6	190 ± 6	191 ± 5	225 ± 11	93 ± 3	186 ± 15	190	202 ± 8
Zr	113 ± 3	117 ± 3	114 ± 3	115 ± 3	137 ± 3	183 ± 8	152 ± 3	111 ± 14	116	180 ± 14
Rb/Zr	1.04 ± .06	.98 ± .07	1.02 ± .04	1.01 ± .05	.88 ± .06	.58 ± .04	.81 ± .04	1.14 ± .16	∿ .97	.66 ± .08
Sr/Zr	1.67 ± .06	1.64 ± .08	1.65 ± .06	1.65 ± .06	1.39 ± .05	1.23 ± .08	.61 ± .02	1.68 ± .25	∿1.64	1.12 ± .10

a) In order to compare the data of Zeitlin and Heimbuch with LBL measurements, the Z & H data were modified as follows: Rb = (Z & H value) * 1.01 - 25, Sr = (Z & H value) * 1.12 - 25, Zr = (Z & H value) * 1.43 - 25. In addition, 15% of the Sr was removed from the Zr value. The errors are the maximum of the square root of the pooled sources variance given by Z & H or the root-mean-square direction in the calibration coefficient used to intercalibrate the two laboratories. These latter are 5%, 4% and 8% for Rb, Sr and Zr respectively.

b) In order to compare the data of Cobean with LBL measurements, the Cobean data were modified as follows: Rb = (Cobean mean Rb) * .9, Zr = (Cobean mean Zr) * 1.23 - .15 * (Cobean mean Sr). Cobean's lower Sr limits were taken as 5 rather than 30 ppm.

c) "Jilotepeque" obsidian as measured by Z & H cannot be distinguished from Las Burras obsidian as measured in the present work.

Table 2.

Chimaltenango Obsidian Abundances[a] Measured by Neutron Activation Analysis

					Other Workers		
					Hurtado de Mendoza et al[d]		Jack[d]
	Representative[b] Rio Pixcayá	Las Burras	Sauces	Odd Sample From Rio Pixcayá Riverbed	San Martin Jilotepeque	Pixcayá	Rio Pixcayá
No. of Samples	8	1	1	1	4	4	1
Al%	7.03 ± 0.20						
Ba	1105 ± 32	1096 ± 17	1042 ± 21	1074 ± 31			1000
Ce	47.5 ± 0.3	51.5 ± .7	47.2 ± .6		47	48	∿40
Co	0.38 ± 0.6	0.57 ± .05	.63 ± .05				
Cs	3.37 ± 0.12	2.24 ± .06	3.70 ± .08		4.2	3.8	
Dy	2.03 ± 0.10	2.49 ± .12	2.42 ± .15	3.35 ± .09			
Eu	0.543 ± 0.10	.708 ± .009	.594 ± .010				
Fe%	0.655 ± 0.018	.899 ± .011	.758 ± .010		.78	.65	.65
Hf	3.21 ± 0.10	4.71 ± .07	3.65 ± .06				
K%	3.54 ± 0.25	3.26 ± .35	3.18 ± .34	3.24 .31			3.4
La	26.3 ± 0.5	27.1 ± .5	25.8 ± .5				∿25
Mn[c]	521 ± 10	626 ± 6	589 ± 6	554 ± 6			
Na%	2.94 ± 0.05	3.33 ± .03	3.15 ± .03	3.42 ± .03			
Rb	122 ± 6	118 ± 5	118 ± 4		120	115	129
Sb	0.37 ± 0.05	.31 ± .04	.46 ± .06				
Sc	1.99 ± 0.03	2.031 ± .020	2.112 ± .021		2.12	1.99	
Sm	2.69 ± 0.03	3.170 ± .032	2.839 ± .028				
Ta	0.757 ± 0.008	.683 ± .007	.751 ± .008				
Th	9.24 ± 0.12	7.33 ± .07	9.21 ± .09		9.6	9.4	∿5
U	2.81 ± 0.05	2.264 ± .028	2.971 ± .033				
Yb	1.403 ± 0.025	1.759 ± .029	1.676 ± .025				
Comment:					Like Sauces	Like Representative Rio Pixcayá	Like Representative Rio Pixcayá

(a) The errors are the larger of the counting error or (if more than one sample) the root-mean-square deviation.

(b) This group includes 2 samples from the riverbed, 4 from Finca Durazno and 2 from a road cut (outcrop 3-1 as designated by Sidrys).

(c) Recalibrated Z & H Mn values for Aldea Chatalun and Jilotepeque are 496 ± 50 and 561 ± 56 respectively. The recalibration formula was Mn = (Z & H value) * (.82 ± .08).

(d) Hurtado de Mendoza and Jester's gamma ray counting rate data were changed to ppm or % by multiplying their Ce, Cs, Fe, Rb, Sc (1121 Kev) and Th values by 1.79, .45, .229, 61, .165 and .45 respectively. This calibration is crude and assumes these Cerro Chayal obsidian group is like our El Chayal Village - La Joya obsidian group.

(e) These are XRF measurements by R. N. Jack. They are included in a summary by Stross et al, 1976.

Table 3.

Element Abundances of Obsidian from San Bartolomé Milpas Altas in Sacatepequez

	Finca Nimachay (this work)	Stross et al - 1976 (see reference e Table 2)	Zeitlin & Heimbuch (Revised)[c]	Cobean (Revised)[d]	Finco Matilandia Hurtado de Mendoza & Jester (Revised)[e]
Al(%)	6.71 ± .10[a]				
Ba	1116 ± 14	1100			44
Ce	42.4 ± .6	~40			
Co	.62 ±.05				
Cs	3.43 ± .07				3.7
Dy	2.15 ± .08				
Eu	.523 ± .009				
Fe(%)	.828 ± .011	.84			.78
Hf	4.09 ± .06				
K(%)	3.48 ± .23	3.3			
La	21.4 ± .5	~20			
Mn	497 ± 10	535	493 ± 40	~465	
Na(%)	3.15 ± .06				
Rb	139 ± 5	115	132 ± 11	~128	131
Sb	.25 ± .04				
Sc	2.258 ± .023				2.20
Sm	2.525 ± .025				
Sr	128 ± 4[b]	115	132 ± 8	~125	
Ta	.593 ± .006				
Tb	9.77 ± .10	~15			10.3
U	3.21 ± .04				
Yb	1.649 ± .024				
Zr	149 ± 4[b]	125	153 ± 12	~144	

(a) Abundances are expressed in ppm or, if indicated after the chemical symbol, in %. The indicated errors in the Finca Nemachay measurements are counting errors.

(b) Measured semi-quantitatively by XRF. These are calibration uncertainties besides the counting errors.

(c) See footnote a of Table 1.

(d) See footnote b of Table 1.

(e) See footnote d of Table 2.

ACKNOWLEDGMENTS

We thank Professor Payson Sheets of the University of Colorado at Boulder for contributing most of the obsidian sources from Chimaltenango analyzed in this work. More detailed discussions of these samples are appearing in the reports on the excavations in which he has participated under the auspices of the University of Pennsylvania Museum.

FOOTNOTE AND REFERENCES

*Work on Mesoamerican obsidian has been funded by the University of Colorado at Boulder, the University of Texas at San Antonio, the University of Pennsylvania, and the U.S. Department of Energy.

1. R. Sidrys, J. Andresen, and D. Marcucci, "Obsidian Sources in the Maya Area," J. New World Archaeology 1 (5):1-13 (1976).

2. R. H. Cobean, M. D. Coe, E. A. Perry, Jr., K. K. Turekian, and D. P. Kharkar, "Obsidian Trade at San Lorenzo Tenochtitlan, Mexico," Science 174:666-671 (1971).

3. F. Asaro, H. V. Michel, R. Sidrys, and F. H. Stross, "A High-Precision Chemical Characterization of Major Obsidian Sources in Guatemala," Am. Antiquity 43:436-443 (1978).

4. F. H. Stross, F. Asaro, H. V. Michel, and R. Gruhn, "Sources of Some Obsidian Flakes from a Paleo-indian Site," Am. Antiquity 42:114-118 (1977).

5. F. Asaro, F. H. Stross, R. Sidrys, and H. V. Michel, Energy and Environment Division Annual Report 1978, Lawrence Berkeley Laboratory report, LBL-8619, p. 291-293.

6. R. N. Zeitlin, and R. C. Heimbuch, "Trace Element Analysis and the Archaeological Study of Obsidian Procurement in Precolumbian Mesoamerica," Lithics and Subsistence -- The Analysis of Stone Tool Use in Prehistoric Economics, (D. Davis, ed.) Vanderbilt University, Publications in Archaeology #20 (1978).

7. L. Hurtado de Mendoza and W. A. Jester, "Obsidian Sources in Guatemala: A Regional Approach," Am. Antiquity 43:424-435 (1978).

8. F. H. Stross, T. R. Hester, R. F. Heizer, and R. N. Jack, "Chemical and Archaeological Studies of Mesoamerican Obsidian," Advances in Obsidian Glass Studies, (R. E. Taylor, ed.), Noyes Press (1976).

This report was done with support from the Department of Energy. Any conclusions or opinions expressed in this report represent solely those of the author(s) and not necessarily those of The Regents of the University of California, the Lawrence Berkeley Laboratory or the Department of Energy.

Reference to a company or product name does not imply approval or recommendation of the product by the University of California or the U.S. Department of Energy to the exclusion of others that may be suitable.

TECHNICAL INFORMATION DEPARTMENT
LAWRENCE BERKELEY LABORATORY
UNIVERSITY OF CALIFORNIA
BERKELEY, CALIFORNIA 94720